The control of alternative splicing by SRSF1 in myelinated afferents contributes to the development of neuropathic pain

[1,2]Richard P. Hulse, [2]Robert A.R. Drake, [1,2]David O Bates, [2,3]Lucy F. Donaldson

Author affiliations:

[1]Cancer Biology, School of Medicine, University of Nottingham, Nottingham, NG7 7UH, [2]School of Physiology and Pharmacology, University of Bristol, University Walk, Bristol BS8 1TD, United Kingdom; [3]School of Life Sciences and Arthritis Research UK Pain Centre, University of Nottingham, Nottingham, NG7 7UH.

***Corresponding authors:**

Dr. R.P. Hulse

Email: Richard.Hulse@nottingham.ac.uk

Tel: + 44 115 823 1307

Dr. L.F. Donaldson

Email: Lucy.Donaldson@nottingham.ac.uk

Tel: +44 115 823 0158

Highlights

- Regulation of SRPK1 (Serine Arginine-rich Protein Kinase 1)-SRSF1 (Serine Arginine-rich Splicing Factor 1) mediated alternative RNA splicing in the spinal cord modulates neuropathic pain.
- SRSF1 is located in myelinated sensory afferent terminals.
- Vascular Endothelial Growth Factor-A (VEGF-A) expression regulates chronic pain at the level of the spinal cord.

Abstract

Neuropathic pain results from neuroplasticity in nociceptive neuronal networks. Here we demonstrate that control of alternative pre-mRNA splicing, through the splice factor serine-arginine splice factor 1 (SRSF1), is integral to the processing of nociceptive information in the spinal cord.

Neuropathic pain develops following a partial saphenous nerve ligation injury, at which time SRSF1 is activated in damaged myelinated primary afferent neurons, with minimal found in small diameter (IB_4 positive) dorsal root ganglia neurons. Serine arginine protein kinase 1 (SRPK1) is the principal route of SRSF1 activation. Spinal SRPK1 inhibition attenuated SRSF1 activity, abolished neuropathic pain behaviors and suppressed central sensitization. SRSF1 was principally expressed in large diameter myelinated (NF200-rich) dorsal root ganglia sensory neurons and their excitatory central terminals (vGLUT1+ve) within the dorsal horn of the lumbar spinal cord.

Expression of pro-nociceptive VEGF-A_{xxx}a within the spinal cord was increased after nerve injury, and this was prevented by SRPK1 inhibition. Additionally, expression of anti-nociceptive VEGF-A_{xxx}b isoforms was elevated, and this was associated with reduced neuropathic pain behaviors. Inhibition of VEGF receptor-2 signaling in the spinal cord attenuated behavioral nociceptive responses to mechanical, heat and formalin stimuli, indicating that spinal VEGF receptor-2 activation has potent pro-nociceptive actions. Furthermore, intrathecal VEGF-A_{165}a resulted in mechanical and heat hyperalgesia, whereas the sister inhibitory isoform VEGF-A_{165}b resulted in anti-nociception. These results support a role for myelinated fiber pathways, and alternative pre-mRNA splicing of factors such as VEGF-A in the spinal processing of

neuropathic pain. They also indicate that targeting pre-mRNA splicing at the spinal level could lead to a novel target for analgesic development.

Keywords

VEGF-A, SRPK1, SRSF1, myelinated, spinal cord, neuropathic pain

Abbreviations

VEGF-A = Vascular Endothelial Growth Factor – A

SRSF1 = Serine Arginine-rich Splicing Factor 1

SRPK1 = Serine Arginine-rich Protein Kinase 1

VEGFR2 = Vascular Endothelial Growth Factor Receptor 2

PSNI = Partial Saphenous Nerve Ligation Injury

Introduction

Insults to the peripheral nervous system usually result in pain and hypersensitivity to noxious (hyperalgesia) and innocuous (allodynia) stimuli. These abnormal sensations arise due to neuronal plasticity leading to alterations in sensory neuronal excitability. These alterations include peripheral sensitization [20], with enhanced evoked and on-going activity in primary afferents, and central sensitization, responsible for the generation and maintenance of chronic pain. The most widely accepted model for establishment of central sensitization is that ectopic firing/increased activity in C-nociceptive afferents drives altered spinal sensory processing, particularly the processing of A-fiber inputs, resulting in secondary hyperalgesia and allodynia (pain remote from an area of damage) [46,89,90] [42,74,97]. C-nociceptor changes are reported in the majority of studies of animal or human neuropathies [1,14,20,38,40,68-70,96] (although not all e.g. [14,38]). Central sensitization can also occur through neuro-immune interactions, following injury-induced local immune cell infiltration and cytokine production/release [80]. After nerve injury there is activation of spinal glia, disruption of the blood-spinal cord barrier, and consequent infiltration of immune cells [16]. These events can alter the central processing of peripheral inputs, implicated in the development of chronic pain [27,39,76]. There is, however still debate on how the processing of A or C fiber inputs is differentially regulated to form the neuronal basis of chronic pain.

During chronic pain, changes in the complement of proteins result in alterations in sensory neuron excitability, as recently demonstrated whereby expression of voltage gated potassium channels in the DRG is altered in ATF3 positive sensory neurons following nerve injury [79]. Furthermore, alternative mRNA splicing allows for functionally distinct proteins to arise from a single gene. This provides a vast repertoire

of actions from a limited source of transcripts, allowing for cell-specific and stimulus-induced alteration in cellular function. Targeting regulation and expression of alternative RNA transcripts, and hence proteins, has been proposed as a potential route for novel drug discovery [73], but this has not been widely investigated with respect to nociception/analgesia.

We recently demonstrated the analgesic effect of targeting alternative mRNA splicing, by inhibition of peripheral serine-arginine rich protein kinase 1, SRPK1 [35]. SRPK1 controls phosphorylation of serine-arginine rich splice factor 1 (SRSF1), which is fundamental to the control of the vascular endothelial growth factor A (VEGF-A) family alternative splicing [2,8,59,60]. Inactive SRSF1 is located in the cytoplasm, but when phosphorylated by SRPK1 it translocates to the nucleus. There are two VEGF-A isoform families, VEGF-A_{xxx}a and VEGF-A_{xxx}b [31] where xxx refers to the number of amino acids encoded, and a and b denote the terminal amino acid sequence. SRSF1 phosphorylation results in preferential production of the proximal splice site isoforms, VEGF-A_{xxx}a [59]. Little is understood about the contribution of VEGF-A proteins to nociceptive processing. VEGF receptor-2 (VEGFR2), the principal receptor activated by both isoform families, has been implicated in nociceptive processing in animal [29,35,50], and clinical studies [43]. VEGF-A isoforms and VEGFR2 are present in the spinal cord [6], and contribute to neuroregeneration and neuroprotection [83].

We therefore tested the hypothesis that the SRPK1/SRSF1 system contributes to spinal nociceptive processing in rodent models of neuropathic pain, concentrating on the effects of SRPK1 inhibition, and VEGF-A_{xxx}a/VEGFR2 signaling in central terminals of myelinated afferents.

Materials and Methods

Animals

Adult male Wistar rats (total 72; 250-350g, Harlan UK) and adult male 129Ola mice (total 20; 25-30g inbred strain) were used. Animals were provided food and water ad libitum. All animal procedures were carried out in laboratories at the University of Bristol in accordance with the U.K. Animals (Scientific Procedures) Act 1986 plus associated U.K. Home Office guidance, EU Directive 2010/63/EU, with the approval of the University of Bristol Ethical Review Group.

Nociceptive Behavior

Nociceptive behavioral testing was carried out as previously described [35]. All animals were habituated to both handling by the tester and the testing environment on the day prior to testing. Two days of baseline testing were carried out prior to any intervention (either drug or surgical) followed by testing post-intervention at discrete time-points as detailed in each experiment. Stimuli were applied to the partially innervated medial aspect of the plantar surface of the hindpaw, an area innervated by the saphenous nerve. Mechanical withdrawal thresholds were calculated from von Frey hair force response curves. Animals were housed in Perspex holding chambers with metal mesh floors (Ugo Basile) and allowed to habituate for 10 minutes. A range of calibrated von Frey hairs were applied to the plantar surface of the hindpaw (for a maximum of five seconds or until paw withdrawal), with a total of five applications per weighted hair. From these data, force response curves were generated and withdrawal values were calculated as the weight at which withdrawal frequency = 50%. Tactile allodynia was assessed in the metal mesh floored enclosures using a brush moved

across the plantar surface of the hindpaw where a withdrawal scored one, with no response zero. This was repeated a total of five times giving a maximum score of five per session. Cold allodynia: a single drop of acetone was applied to the plantar surface of the hindpaw using a 1ml syringe a maximum of five times giving a maximum score of five if the animal exhibited licking/shaking behavior in response to each application. Thermal hyperalgesia (Hargreaves test[30]): animals were held in Perspex enclosures with a glass floor. A radiant heat source was positioned under the hindpaw, and the latency was recorded for the time taken for the animal to move the hindpaw away from the stimulus. This was repeated three times and a mean value calculated for each test.

Formalin Testing: animals were habituated to glass floored testing enclosures as above. A single 50µl injection of 5% formalin was administered to the plantar surface of the right hindpaw by intradermal injection. Immediately following formalin injection, animals were placed into the testing enclosures. Time (seconds) spent exhibiting pain-like behaviors and the total number of pain-like behaviors was recorded in five minute bins for sixty minutes. Data are shown as the classical biphasic response with behavioral responses pooled for the first phase 0-15 minutes and second phase 20-60 minutes. Blinding of nociceptive behavioural studies are routine in the laboratory however where animal welfare/experimental design prohibits this, it cannot be implemented. For instance, in nerve-injured animals blinding is not possible as controls are naïve. The lack of blinding may have introduced some subjective bias into these experiments, which is in part mitigated by behavioural data is supported by the inclusion of experiments in which measurements are not subjective (e.g. *in vivo* noxious e.m.g. recording, expression analysis, and neuronal activation using c-fos).

Electromyographic Experiments

A well-defined method for minimally invasive preferential selection of either C- or A-fibre mediated nociceptive pathways was used [93,94]. Noxious withdrawal responses to A- and C-nociceptor selective stimulation were carried out as previously described [44,45,53], by measurement of electromyographic activity in biceps femoris. Animals were anaesthetized using isoflurane induction (4% in oxygen), and the external jugular vein and trachea were cannulated to allow maintenance of airway and anesthesia. Following surgery, anesthesia was switched to alfaxalone (~30mg/kg/hr i.v.), and animals were maintained at a steady level of anesthesia by continuous pump perfusion via the jugular vein for the remainder of the experiment. Bipolar electrodes were made with Teflon coated stainless steel wire (Advent Research Materials, Oxford UK) implanted into the bicep femoris. EMG recordings were amplified and filtered by a combination of in-house built and Neurolog preamplifier and band pass filters (Digitimer Neurolog System). Animals were maintained at a depth of anesthesia where a weak withdrawal to noxious pinch could be elicited for the duration of the experiment. A- and C-cutaneous nociceptors were preferentially activated to elicit withdrawal reflex EMGs using a well-characterized contact heating protocol [44,45,53]. Two different rates of heating (2.5^{O}C/s and 7.5^{O}C/s) were applied to the dorsal surface of the left hindpaw as these are known to preferentially activate slow/C-nociceptors (2.5^{o}C$\cdot$s^{-1}) and fast/A nociceptors (7.5^{o}C$\cdot$s^{-1}) respectively. Contact skin temperature at the time of onset of the EMG response was taken as the threshold. A cutoff of 58^{o}C for A-nociceptors, 55^{o}C for C-nociceptors was put in place to prevent sensitization if no response was elicited. If a withdrawal response was not elicited, threshold was taken as cut-off +2^{o}C [22]. Three baseline recordings were performed before i.t. drug injection with a minimum 8 minutes inter-stimulus interval, and alternating heating rates, to prevent sensitization or damage to the paw. Digitized data acquisition, digital

to analogue conversion, and offline analyses were performed using a CED Micro1401 Mark III and Spike2 version 7 software (Cambridge Electronic Design, UK).

Nerve injury model

The partial saphenous nerve ligation injury (PSNI) model was used to induce mechanical and cold allodynia, as described previously [34,84]. Under isoflurane anesthesia (3% in $O_{2,}$), the saphenous nerve was exposed via an incision made along the inguinal fossa region of the right hind leg. Approximately 50% of the nerve was isolated and tightly ligated using 4.0 silk suture, and the incision was closed using size 4.0 sterile silk suture.

Drugs and drug delivery

I.t. injections were carried out under isoflurane (4% in oxygen) anesthesia, using 0.5ml insulin syringes (29 gauge, Terumo) in rats and mice. For i.t. administration, 10 µl injections were made in the midline of the vertebral column through the intervertebral space between lumbar vertebrae five and six. The injection was deemed to be in the correct place when it evoked a tail flick response. Rats were used for i.t. anti-VEGF-A_{xxx}b experiments, as the 56/1 mouse monoclonal antibody had not been validated in mice at that time. All nociceptive behavioural testing was carried out one hour after intrathecal injection as initial experiments indicated that responses to i.t. PTK peaked at 1 hour, and returned to normal by 2 hours after injection.

All drugs were made up as stock concentrations and then diluted to working concentration in phosphate buffered saline (PBS) as described in each experiment. Vehicle controls were used for each drug. PTK787 (LC laboratories, USA) was dissolved in polyethylene glycol (PEG) 300/PBS, with the final PEG 300 concentration

at 0.002%. ZM323881 (Tocris, UK) was made up in DMSO/PBS and given intrathecally at a final concentration of 100nM ZM323881/0.001% DMSO. Mouse monoclonal VEGF-A_{165}b antibody 56/1 (AbCam ab14994; MRVL56/1), recombinant human (rh)VEGF-A_{165}A (R&D systems, UK) and rhVEGF-A_{165}b (R&D Systems UK) were all dissolved in PBS. SRPIN340 (N-[2-(1-piperidinyl)-5-(trifluoromethyl)phenyl] iso nicotinamide; SRPK inhibitor [25] purchased from Ascent Scientific, Bristol, UK) was dissolved in DMSO and diluted to final concentrations in PBS (to a final DMSO concentration of 0.03%). All peptides and concentrations used have been previously shown to exert functional effects in neurons and/or other biological systems [9,35,63]. SRPIN340 has been used in several other studies, different pathological states, and was used at a known functional concentration (10μM), as previously described [2,35,51].

Immunohistochemistry

Rats were terminally anesthetized with sodium pentobarbital overdose (i.p. 60mg/kg) and were perfused transcardially with saline followed by 4% paraformaldehyde. The L3-4 segments of the lumbar enlargement, containing the central terminals of saphenous nerve neurons [64], and L3-L4 dorsal root ganglia were removed, post fixed in 4% paraformaldehyde for 2 hours and cryoprotected in 30% sucrose for 12 h. Tissue was stored in OCT embedding medium at -80^{o}C until processing. A cryostat was used to cut spinal cord (20μm) and dorsal root ganglia (8μm) sections that were thaw mounted onto electrostatic glass slides. Slides were washed in phosphate buffered saline (PBS) solution 3 times for 5 minutes per incubation, and incubated in PBS 0.2% Triton X-100 for 5 minutes. Sections were blocked (5% bovine serum albumin, 10% fetal bovine serum, 0.2% Triton X-100 in PBS) for 2 hours at room temperature, and then incubated in primary antibodies diluted in blocking solution

overnight at 4^{o}C. Sections were washed three times in PBS washes and incubated for 2 h in secondary antibody (e.g. biotinylated or alexafluor-conjugated; 0.2% Triton X-100 in PBS). For the third stage (i.e. streptavidin-alexfluor conjugate), incubations and washes were as described for the secondary antibody. Slides were washed in PBS 3 times prior to coverslipping in Vectorshield (H1000 or H1200 containing DAPI for nuclear staining, Vector Laboratories). Images were acquired on either Nikon Eclipse E400 and a DN100 camera or Leica TCS SPE confocal microscope using Leica application suite (Tumor and Vascular Biology Laboratories' imaging suite UoN).

Primary antibodies used were as previously reported [2,59]: anti-ATF3 (rabbit polyclonal; 2µg/ml: Santa Cruz), anti-c-fos (rabbit polyclonal; 2µg/ml: Santa Cruz), anti-SRSF1 (goal polyclonal; 2µg/ml; sc-10255 Santa Cruz), anti-vGLUT1 (rabbit polyclonal, 60pg/ml, Synaptic Systems), anti-NF200 (mouse monoclonal; 1.4µg/ml; N0142 Sigma-Aldrich), anti-NeuN (mouse monoclonal, 1 in 100, Millipore). Use of anti-VEGF-A and SRSF1 antibodies for both immunolocalisation and immunoblotting has been previously reported [2,8]. Secondary antibodies (1 in 1000 dilution and from Invitrogen unless stated): Alexafluor 488 goat anti-mouse, Alexafluor 488 chicken anti-goat, Alexafluor 555 donkey anti-goat, Alexafluor 555 donkey anti-rabbit; biotinylated anti-rabbit (Stratech Scientific), Extravidin CY3 (Sigma-Aldrich). Dorsal root ganglia neuronal cell counts were performed using ImageJ analysis to measure neuronal area (µm^2) [67]. The saphenous nerve is approximately equally derived from lumbar DRGs 3 and 4 in rat and human [5,64,95]; the mean number of neurons per section was quantified from 10 non-sequential random L4 DRG sections per animal. Data are presented as the mean number of neurons per section and the experimental unit is the animal. The number of activated SRSF1-positive neurons (defined as those showing nuclear localization of SRSF1) was calculated as a percentage of total

neurons as designated by size (small<600μm^2, medium 600μm^2-1200μm^2, large>1200μm^2) [79]. The total number of DRG neurons quantified was ~5000 (100 neurons per section, 10 per animal, 3 per group). Determination of SRSF1 spinal cord expression/localization was determined from 5 non-sequential random spinal cord sections per animal using Image J analysis. Images were converted to an 8-bit/grayscale image then thresholding was applied across all acquired images to determine the area of positive staining. Areas of positive staining were then quantified across all sections and groups. Colocalisation was determined via coloc2 plugin in ImageJ. Controls for VEGF-A and SRSF1 immunofluorescence consisted of incubation with only secondary antibody ('no primary' control) or substitution of the primary antibody with a species matched IgG.

Western blotting

Naïve and PSNI rats (treated with i.t. vehicle or SRPIN340) were terminally anesthetized (i.p. 60mg/kg sodium pentobarbital) and perfused with saline solution. The lumbar region of the spinal cord was extracted and frozen immediately on dry ice, then stored at -80^{o}C. Protein lysates (80μg/well) were prepared using lysis buffer (RIPA buffer, Sigma-Aldrich) with protease inhibitors (Sigma-Aldrich) and samples were homogenized. Protein extracts were stored at -80^{o}C until required. Samples were run on a 4% stacking gel/12 % running SDS-PAGE gel (90V, 1hr 30min) and transferred (wet transfer) to nitrocellulose membrane for 1hr @ 100V. Membranes were then incubated with either α-SRPK1 (mouse; 1μg/ml; Sigma-Aldrich), α-SRSF1 (ASF/SF2; rabbit; 0.5μg/ml; Abcam), α-SRSF1 (ASF/SF2; mouse; 0.5μg/ml; SantaCruz), α-Actin (SantaCruz; 2μg/ml) α-VEGF-A_{165}b (mouse; 4μg/ml; Abcam;), α-pan-VEGF-A (rabbit; Santa Cruz A20; 2μg/ml) or α-tubulin (mouse; 1 in 4000; Sigma-Aldrich) antibodies and visualized with Femto chemoilluminescence kit (exposure

between 1 second and 1 minute,Thermo Scientific) or Licor IRdye secondary antibodies (as previously reported [2,25,59])

Statistical Analysis

All data are represented as means ± SEM. Data were extracted and analyzed using Microsoft Excel 2010, Graphpad Prism v6 and ImageJ [67]. Nociceptive behavioral analyses were between-subjects designs comparing effects of drugs by two way ANOVA with post-hoc Bonferroni tests. In those experiments involving intrathecal and intraperitoneal administration of drugs in naïve animals, both hind paws were included in the analysis as replicates. EMG experiments used a within-subjects design and immunofluorescence experiments a between-subjects design with the effects of drug treatment compared to baseline values using one-way ANOVA with post-hoc Bonferroni tests. Immunofluorescence analysis of spinal cord (c-fos quantification) was taken from entirety of dorsal horn. DRG (SRSF1+ve) and spinal cord (c-fos) neuron counts were ascertained from multiple representative images, at least 10 per animal and the mean value of those 10 calculated. Coloc2 analysis (Image J plugin) was used to ascertain the pixel intensity spatial correlation (co-localization) of SRSF1 and vGLUT1 staining in the spinal cord. This provides an automated measure of the correlation of pixel intensity for the two independent immunofluorescence channels for each sample, given as the Pearson's correlation co-efficient [17,47]. Western blot analyses of SRSF1 and VEGF-A family expression were determined from ImageJ densitometry analysis (gel analysis plug in) and compared using Mann Whitney U tests. All F test statistics are described as a column factor with reference to drug/experimental grouping. NS designates not significant.

Results

SRSF1 is predominantly expressed in myelinated neurons in rats

SRPK1 and SRSF1 are key factors in the control of VEGF-A_{xxx}a preferential splicing particularly in disease [2,59]. SRSF1 is expressed in the cytoplasm of dorsal root ganglia (DRG) neurons in naïve animals [35](Fig. 1A-C). Upon activation (phosphorylation), SRSF1 is known to translocate from the cytoplasm to the nucleus [2,59], where it is involved in pre-mRNA processing. Following PSNI, SRSF1 immunoreactivity in sensory DRG neurons was found to be nuclear (Fig. 1E-G) in some but not all neurons. Matched IgG (Fig. 1D) and omission of primary antibody (Fig.1H) controls showed no signal. PSNI injury induces activating transcription factor 3 (ATF3) expression in injured DRG sensory neurons [9]. There was an increase in ATF3-positive DRG neurons after PSNI (Fig. 1I-K), with 43% of DRG neurons expressing ATF3 post-PSNI compared to only 1% in naïve animals (Fig. 1K). After PSNI, all nuclear localized SRSF1-positive (Fig 1L) DRG neurons (Fig 1M) were also ATF3 positive (Fig 1N), indicating nuclear SRSF1 was exclusively found in damaged neurons (Fig. 1O). This represents that 45% of ATF3 -positive neurons were also SRSF1 positive, with the remaining 55% of ATF3 positive neurons negative for SRSF1.

SRSF1 was expressed predominantly in the cytoplasm of 96% of larger (cross sectional area >1200µm^2) neurofilament-200 (NF200) positive DRG neurons in naïve animals (Fig. 2A-C, L), and 71% of medium (area 601-1200 µm^2) neurons, but was in only a small proportion (14%) of neurons of area <600 µm^2 (small, <30µm diameter). NF200 is a marker for myelinated neurons indicating that SRSF1 expression is principally found in the somata of A-fiber DRG neuronal population, but it was also

found in peripheral sensory nerve fibers in PSNI animals (Fig. 2I-K). Following PSNI, activated (nuclear) SRSF1 co-localized with ATF3 and NF200 in DRG sensory neurons (Fig. 2D-F), The size distribution of activated (nuclear) SRSF1 in injured neurons was similar to that in naives, - 69% of large cells, 21.5% of medium cells but a small proportion (1.7%) of small neurons. In contrast, only a minority of the IB4-binding, largely unmyelinated DRG neurons from nerve-injured animals were positive for SRSF1 (Fig. 2G-H). The size distribution profile of DRG sensory neurons indicated that SRSF1-positive neurons are medium/large in size (Fig. 2L).

SRSF1 immunofluorescence was also identified in the lumbar region of the spinal cord of PSNI rats, where it was co-localized with the marker of myelinated primary afferent central terminals, the vesicular glutamate transporter 1 (vGLUT1, Fig. 3A-C) [11,58,92]. There was an increase in SRSF1 expression in the central sensory terminals 2 days after PSNI, as assessed by immunofluorescence (Fig. 3D-I) and quantified by Western blot (Fig. 3J-K; $p=0.055$). Co-localization analysis of vGLUT1 and SRSF1 staining showed a stronger colocalization in the PSNI animals (indicative of increased SRSF1 expression) in PSNI (Fig. 3L). vGLUT1 is found in large diameter myelinated neurons, and is not found in either the peptidergic or IB_4-binding C-nociceptor populations [11,62]. Furthermore, SRSF1 (Fig. 3M) was co-localized with vGLUT1 (Fig. 3M-O) in DRG sensory neurons. There was no SRSF1 expression in the contralateral dorsal horn of either naïve or PSNI rats, although vGLUT1 expression was evident, indicating that the increased spinal SRSF1 expression was associated with injury to peripheral neurons and not a systemic response (Fig. 3P-S).

Attenuation of SRSF1 mediated alternative splicing prevents A-nociceptor mediated neuropathic pain in rats

The increased SRSF1 immunoreactivity in vGLUT1-positive central terminals after PSNI (Fig. 3) was accompanied by an increase in total VEGF-A expression in spinal cord (Fig. 4A-F) assessed with the pan-VEGF-A antibody A20 [2]). VEGF-A was also co-localized with SRSF1 in some, but not all central terminals (Fig. 4G-I). VEGF-A_{xxx}b remained unchanged in spinal cord after PSNI whereas total (pan)-VEGF-A significantly increased (Fig. 4J&K). This indicates an increase in the expression of VEGF-A_{xxx}a isoforms, resulting in a decrease in VEGF-A_{xxx}b as a proportion of total-VEGF-A (Fig. 4L).

These results suggest that SRSF1 phosphorylation and activation at the level of the spinal cord is induced by PSNI, and is accompanied by a change of the balance of VEGF isoforms toward VEGF-A_{xxx}a. As VEGF-A_{165}a has been shown to be pro-nociceptive, and VEGF-A_{165}b anti-nociceptive [35], it is therefore possible that changes in SRSF1 and VEGF-A expression at the level of the spinal cord are associated with the development of neuropathic pain behaviors. SRSF1 activity is activated through phosphorylation by serine-arginine-rich protein kinase SRPK1 [2]. To test the hypothesis that PSNI neuropathic pain is dependent upon SRSF1 activation, we inhibited SRPK1 in the spinal cord of rats, with intrathecal (i.t) injection of the SRPK1 antagonist, SRPIN340 (N-[2-(1-piperidinyl)-5-(trifluoromethyl)phenyl] isonicotinamide, Ascent Scientific, Bristol UK) [24] (10µM i.t. injection) at the time of nerve injury surgery (time point day 0). SRPIN340 has been used extensively to inhibit SRPK1 activity and a multitude of studies have demonstrated its involvement with controlling alternative splicing for VEGF-A isoforms [2,51,59], through suppression of SR protein phosphorylation and stabilization [24]. SRPIN340 inhibits both SRPK1 and

SRPK2 at concentrations equal or less than 10μM [24], and this has been shown previously to inhibit VEGF-A_{xxx}a production *in vitro* [59] and *in vivo* [2]. PSNI induced a reduction in mechanical withdrawal thresholds in the ipsilateral hindpaw as expected, and this was blocked by i.t. SRPIN340 (Fig. 5A; PSNI+vehicle n=9, PSNI+SRPIN n=6). Tactile and cooling allodynia which also developed in the ipsilateral hindpaw (Figs. 5B & C) were also inhibited by SRPIN340. Contralateral hindpaws from vehicle and SRPIN340 treated groups did not differ from each other, indicating no effect of central SRPK1 inhibition on noxious processing from uninjured tissue. The PSNI model does not in itself lead to the development of heat hyperalgesia [34], but Hargreaves latencies did increase as a result of SRPIN340 treatment compared to vehicle treated PSNI animals, both ipsilateral (Fig. 5D) and contralateral (Fig. 5E) to the nerve injury, indicating a possible contribution of SRPK1/SRSF1 in normal nociceptive processing. SRPIN340 treatment also resulted in a significant inhibition of the increase in SRSF1 immunoreactivity in the central terminals of the dorsal horn of the spinal cord induced by PSNI (Fig. 6A-H). Furthermore, the administration of SRPIN340 resulted in increased distal splice site, anti-nociceptive isoform VEGF-A_{xxx}b with no overall change in total VEGF-A expression (Fig. 7A), indicating a switch from proximal to distal splice site transcripts following SRPIN treatment in peripheral nerve injury (Fig. 7B-C). Intrathecal SRPIN340 not only blocked the development of nociceptive behaviors and altered alternative splicing in the dorsal horn, it also blocked indicators of central sensitization. The number of c-fos positive neurons in the spinal cord, a marker of central sensitization [36] as assessed by immunofluorescent staining (Fig. 7D), was increased after PSNI and was significantly reduced by i.t. SRPIN340 (Fig. 7E-F). SRPK1 protein expression within the spinal cord was not significantly altered following nerve injury alone (Fig. 6G)

VEGF-R2 activation at the level of spinal cord contributes to nociceptive processing

VEGF-A_{xxx}a and VEGF-A_{xxx}b differ only in their terminal 6 amino acids. The C-terminal sequence determines the efficacy of VEGFR2 signaling of the isoforms and their functional properties [13]. On binding to VEGFR2, VEGF-A_{xxx}a leads to full phosphorylation and activation of VEGFR2, whereas VEGF-A_{xxx}b activates only partial VEGFR2 phosphorylation, leading to receptor degradation [4]. VEGF-A_{165}b also antagonizes VEGF-A_{xxx}a binding [88]. The different C-terminal sequences also determine the anti- or pro-nociceptive effects of the VEGF-A_{165}b and VEGF-A_{165}a isoforms respectively [35] but both isoforms promote neuroprotection [9,71]. Our findings above show that VEGF-A alternative splicing is altered in neuropathic states (Fig. 3-5), and this is associated with pain behaviors. These results suggest that spinal cord VEGFR2 activation by different VEGF isoforms could contribute to nociceptive processing. Despite evidence from clinical studies that demonstrate an involvement of VEGF receptors in pain [43,52], and experimental evidence showing that spinal VEGF levels are associated with pain [57], there are few published findings on the effects of VEGF-A in spinal nociceptive processing. As spinal VEGF-A splicing and isoform expression, and therefore by inference VEGFR2 activation, were altered in PSNI we determined the effect of VEGFR antagonism on central nociceptive processing.

PTK787 (or vatalanib) is a tyrosine kinase inhibitor that has non-selective inhibitory actions on VEGFR1 and 2. It is 18-fold more selective for VEGFR1 and 2 over VEGFR3, and has slight selectivity for VEGFR2 (IC_{50} <50nM) over VEGFR1 (IC_{50} ~100nM) [86]. In naïve rats, systemic VEGFR antagonism with PTK787 (30mg/kg, i.p.)

increased thermal withdrawal latencies to heat (Fig. 8A n=5/group) indicating an analgesic effect. To determine the effect of PTK787 on one aspect of central nociceptive processing, we used the formalin test. Injection of formalin into the hind paw allows for the investigation of two distinct phases of acute nociceptive behavior. The initial phase (0-15min) is largely mediated by peripheral nerve activation, whereas the second has both a peripheral and central component. One hour prior to formalin injection, rats were treated with either (i.p.) vehicle or PTK787. The acute phase was unaffected (0-15min) by PTK787 treatment (Fig. 8B-E; n=7/group). In contrast the second phase (20-60 min) was significantly reduced by systemic PTK787 treatment for both the time of flinching (Fig. 8B& D) and the number of flinches (Fig. 8C & E). These results suggest a central component of VEGFR inhibition. To determine the targets of VEGF-A/VEGFR signaling in naïve rats, given the effects of the VEGFR antagonist on the second phase of the formalin test, we recorded electromyographic nociceptive withdrawals to selective nociceptor activation. Fast heating (fast heating rates ~7.5^{o}C/s) preferentially activates myelinated A-nociceptors and slow heating activates unmyelinated C-nociceptors, both inducing a withdrawal from the stimulus. To determine VEGFR2 specific actions, ZM323881 (5-[[7-(benzyloxy) quinazolin-4-yl]amino]-4-fluoro-2-methylphenol) was used locally. ZM323881 which has sub-nanomolar potency and specificity for VEGFR2 (IC_{50}<2nM) [85], with an IC_{50} greater than 50μM for VEGFR1 and PDGFR [85]. I.t. ZM323881 (100nM, specific VEGFR2 inhibitor, [85]) led to a prolonged (up to 60 min) increase in the temperature at which the rats withdrew during A-nociceptor stimulation (Fig. 8F, n=3-5 per group). ZM323881 did not have a significant effect on C-nociceptor withdrawals (Fig. 8F). These results show that VEGFR2 signaling is mediated, at last in part, by A-nociceptor activation in the spinal cord.

Taken together, these results are consistent with the hypothesis that the VEGF-A isoforms may have different functions in the spinal cord, as in the periphery [35]. We tested this by giving VEGF agonists and antagonists intrathecally (i.t.), and measuring pain behaviors in mice and rats. PTK787 increased both mechanical withdrawal thresholds (Fig. 9A; n=3 mice/group, 6 hind-paws treated as replicates) and heat nociceptive withdrawal time (Fig. 9B) compared with vehicle treated mice. In contrast injection of 2.5nM VEGF-A_{165}a reduced mechanical withdrawal thresholds (Fig. 9C; n=4 mice/group, 8 hind-paws treated as replicates) and heat withdrawal latencies (Fig. 9D), indicating a central pro-nociceptive action of VEGF-A_{165}a in naïve mice. Conversely, 2.5nM VEGF-A_{165}b increased mechanical thresholds (Fig. 9E n=4 mice group, 8 hind-paws treated as replicates) and heat withdrawal latencies (Fig. 9F) indicating a central anti-nociceptive effect. In rats, administration of a neutralizing antibody against VEGF-A_{xxx}b had a similar effect to that of VEGF-A_{165}a, decreasing withdrawal thresholds to mechanical stimulation (Fig. 9G; n=3 rats group, 6 hind-paws treated as replicates) and the time taken for withdrawal from heat (Fig. 9H), indicating that loss of endogenous VEGF-A_{xxx}b from the spinal cord is painful in naïve animals.

Attenuation of central VEGFR2 signaling leads to alleviation of neuropathic pain

We mimicked the effect of spinal SRPK1 inhibition by increasing the proportion of spinal VEGF-A_{165}b with exogenous protein, 2 days after the onset of neuropathic pain behavior in rats. Intrathecal VEGF-A_{165}b reversed both mechanical (Fig. 10A) and cold allodynia (Fig. 10B) and increased thermal withdrawal latencies both ipsilaterally (Fig. 10C) and contralaterally (Fig. 10D). IP (30mg/kg) PTK787 led to the increase in

withdrawal latencies to heat both ipsilateral (Fig. 10E) and contralateral (Fig. 10F) in PSNI injured rats.

Discussion

We show that the splicing factor kinase SRPK1 is a key regulator of spinal nociceptive processing in naïve and nerve injured animals. We present evidence for a novel mechanism in which altered SRSF1 localization/function in neuropathic pain results in sensitization of spinal cord neurons. Inhibiting the splicing factor kinase SRPK1 can control alternative splicing of VEGF-A isoforms in spinal cord, and can prevent the development of neuropathic pain.

Alternative splicing and pain

The development of neuropathic pain and associated neuronal excitation, results from alterations in neuromodulatory protein function, leading to sensitization of peripheral and central nociceptive systems. Both short and long term changes occur in the expression and function of ion channels, receptors, excitatory and inhibitory neurotransmitters/modulators and second/third messenger systems [15,78,79] leading to the regulation of neuronal excitability through modulation of excitatory and/or inhibitory networks. Many of these alterations can be attributable to altered protein expression (e.g. [61,66]). Alternative pre-mRNA splicing is a rapid, dynamic process, recognised to be important in many physiological processes, including in nociception [37]. Such splicing of many channels and receptors particularly calcium channels, is altered in pain states [3,56], but prior to our studies the control of mechanisms of alternative pre-mRNA splicing had not been considered as a contributory factor in nociceptive processing [35].

Inhibition of SRPK1 alleviates neuropathic pain and reduces SRSF1 activation.

The splicing kinase SRPK1, a member of the serine-arginine-rich kinases, controls alternative pre-mRNA splicing of a relatively small number of identified RNAs [35]. To date, there is strong evidence for the involvement of only one of these, VEGF-A, in nociception [35,49,50,65,83]. SRPK1 controls the activity of splice factor SRSF1 that is fundamental to the processing of pre-mRNA transcripts [28], their cellular localization/transport [10], and it may also be involved in translational repression [19]. Phosphorylation and activation of SRSF1 results in nuclear translocation in a number of cell types [2,59]. After nerve injury activated SRSF1 was only found in the nuclei of injured (ATF-3 positive) large excitatory (vGLUT1 positive) neurofilament-rich DRG neurons whereas it was found in the cytoplasm of uninjured DRG neurons. Interestingly, SRSF1 was also seen in the central terminals of myelinated neurons after injury, but was not in central terminals in naïve animals. The nuclear localization suggests that neuronal SRSF1 is activated in mRNA processing in injured myelinated neurons [2]. The redistribution of cytoplasmic SRSF1 to central terminals may reflect a change in neuronal function or mRNA transport [77]. Little is understood of this function of SRSF1 in sensory neurons, although mRNA transport is closely linked to splicing, and specific mRNA splice variants can be targeted to axons [54].

After traumatic nerve injury, injured DRG neurons (e.g. ATF3 positive) demonstrate ectopic and/or increased evoked activity. These neuronal phenomena arise due to expression changes in key mediators of sensory neuronal excitability, ultimately underlying chronic pain phenotypes [20,79]. Local neuro-immune interactions resulting from damage to neurons alter the properties of adjacent ‘uninjured’ afferents [20,79], including sensitization of A-fiber afferents [96], and together these drive excitability changes in the spinal cord [18]. Mechanisms such as SRPK1/SRSF1-mediated alternative pre-mRNA splicing could underpin this ‘phenotypic switch’

change in properties, for example by controlling relative expression of ion channel splice variants in damaged neurons [3,79]. Increased release of neurotransmitters and modulators from primary afferent central terminals is seen in the spinal cord following nerve injury [26]. The cellular SRSF1 redistribution also suggests that phosphorylated SRSF1 could act to transport RNAs to the central terminals in nerve injury, and hence enable translation of specific isoforms (e.g. VEGF-A_{165}a) in the nerve terminals [26]. This reduction in the amount of SRSF1 present in afferent central terminals following intrathecal SRPK1 inhibition could be due to increased degradation of the SRPK1-SRSF1 complex and/or reductions in transport of mRNA to the central terminals of primary afferents.

In addition to peripheral sensitization, PSNI results in mechanical and cold hypersensitivity [34] and central sensitization [84]. Intrathecal administration of the SRPK1 inhibitor SRPIN340 abolished pain behaviors including mechanical allodynia and hyperalgesia, and cold allodynia, and the central sensitization indicated by spinal c-fos expression. Central hyperalgesic priming of primary afferent nociceptors is dependent on local protein translation in central terminals [23], so we speculate that SRPK1/SRSF1 actions on RNA localization or protein translation [10,19] may also contribute to this sensitization mechanism. As heat hyperalgesia was also reduced but PSNI animals did not display sensitization to radiant heat [33,84], this suggests that central SRPK1 inhibition not only prevents central sensitization, but also reduces activation of non-sensitized spinal nociceptive networks.

VEGF splicing and VEGF-dependent nociceptive processing in spinal cord.

SRPK1/SRSF1 controls the splice site choice in the alternative splicing of the vascular endothelial growth factor A (VEGF-A) family, leading to increased expression of

VEGF-A_{xxx}a isoforms [2,25,59]. VEGF-A_{xxx}a isoforms are widely known as pro-angiogenic/cytoprotective factors and this splicing pathway is strongly associated with solid tumor development [2]. Peripheral administration of VEGF-A_{165}a resulted in pain, as did, somewhat surprisingly, VEGFR2 blockade [35]. These findings are supported by observations that systemic VEGF-A receptor blockers result in pain in clinical studies [12,43] and painful experimental neuropathy [83]. In contrast, given intrathecally, the VEGF-R2 antagonist, PTK787 *decreased* hypersensitivity in naïve and neuropathic rodents (Fig. 8, and [50]), but VEGF-A_{165}a again increased hypersensitivity in naïve (Fig. 8) and spinal cord injury rats [57]. This latter increase in pain was associated with aberrant myelinated fiber sprouting in dorsal horn and dorsal columns that may be VEGF-A dependent [57]. In contrast, van Neervan and colleagues [82] found only very small anti-nociceptive effects of intrathecal VEGF-A_{165}a on pain, and no effect on neuronal function. Observed differences in VEGF-A effects could be attributable to different concentrations used, the source of VEGF-A_{165}a, the degree of injury, or different endogenous isoform complement [6]. Clinically, elevated levels of VEGF-A in the spinal cord of neuropathic pain patients correlate with reported pain [52]. VEGF-A and VEGF-A receptor 2 are present in both peripheral and central nervous systems including spinal cord [7,9,72]. rhVEGF-A_{165}a has consistent pro-nociceptive actions peripherally [35] and centrally, and our findings demonstrate that the different VEGF-A isoform subtypes have opposing actions on nociception in the spinal cord, as they do in the periphery [35]. We are the first to show that the alternatively spliced isoform, VEGF-A_{165}b has anti-nociceptive actions in the spinal cord.

Taken together our observations of: increased spinal splicing factor expression, increased spinal pro-nociceptive VEGF-A_{165}a but unchanged VEGF-A_{165}b expression,

and blockade of pain behavior and VEGF-A expression changes by SPRK1 inhibition, suggest that exogenous and endogenous VEGF-A isoforms modulate spinal nociceptive processing in naïve animals and after peripheral nerve injury. The sites of ligand/receptor expression, the differences in peripheral and central administration, and the current clinical use of many anti-VEGF treatments to treat varied diseases highlight the importance of recognizing the different functions and sites of action of the alternative VEGF-A isoforms.

Myelinated afferents and neuropathic pain.

We found that VEGFR2 blockade resulted in inhibition of A fiber nociceptor-mediated nociception, suggesting that endogenous VEGF is involved in spinal processing of A fiber nociceptor inputs. Irrespective of the animal model or human condition of neuropathic pain, the prevailing evidence is that afferents are sensitized [20,34] both C-fiber [1,14,20,38,40,68-70,96] and A-fiber nociceptors [81,96], increasing the afferent barrage to the spinal cord through enhanced stimulus-evoked responses and/or increases in spontaneous/ongoing firing. Other mechanisms, such as neuro-immune interactions, can also contribute to changes in spinal excitability [80]. The result of increased input to and excitability of spinal neurons is central sensitization [46] leading to hyperalgesia and allodynia. It has been hypothesized that central sensitization allows low threshold A-fiber afferents to “access” pain pathways [48,79] although precise mechanisms are unknown. Early reports of low threshold Aβ fiber mechanoreceptors (LTMs) sprouting into superficial laminae [91] are still debated [32,87]. A-fiber nociceptive afferents, as opposed to LTMs, have similar central terminals in superficial dorsal horn laminae (I and II_o) in both naïve and nerve injured animals [87] and may represent the afferents expressing SRSF1. What is clear is that

altered central processing of myelinated nociceptor information contributes to neuropathic pain [55,75,98], such as secondary dynamic allodynia [41]. Both C-fiber (unmyelinated) and A-fiber (myelinated) pathways can contribute to chronic pain [48,98], but this is the first time that VEGFR2 has been implicated in the processing of information in these pathways. If VEGFR2 is involved in A-fiber nociceptive pathways, then this provides a potential new mechanism for the modulation of nociception.

Conclusion

Here we identify a novel pathway of nociceptive processing through a SRPK1-SRSF1-VEGF-$A_{xxx}a$ axis in myelinated nociceptors that is involved in nociception at the level of the spinal cord. During neuropathic pain development SRPK1 drives expression of pro-nociceptive VEGF-$A_{xxx}a$ at the level of the spinal cord. Therefore the development of SRPK1 targeted therapy, or other controls for alternative splicing, would be interesting targets for novel analgesic agent development [21]. These findings highlight the importance of understanding control of RNA function, including alternative splicing in relation to pain, and considering specific interactions of splice factors in excitatory networks following peripheral nerve trauma.

Acknowledgements

All authors have read and approved final version of the manuscript. RPH, RARD performed research, RPH, DOB & LFD designed the research and analyzed data. RPH, DOB and LFD wrote the manuscript with contributions from RARD and final approval from all authors.

This work was supported by Diabetes UK (11/0004192), the Wellcome Trust (079736) and The Richard Bright VEGF Research Trust (UK Registered Charity 1095785).

LFD and DOB are co-inventors on patents protecting VEGF-A_{165}b and alternative RNA splicing control for therapeutic application in a number of different conditions. LFD and DOB are founder equity holders in, and DOB is director and CSO of Exonate Ltd, a company with a focus on development of alternative RNA splicing control for therapeutic application in a number of different conditions, including diabetic complications. The authors have no other conflicts of interest to declare.

References

[1] Ali Z, Ringkamp M, Hartke TV, Chien HF, Flavahan NA, Campbell JN, Meyer RA. Uninjured C-fiber nociceptors develop spontaneous activity and alpha-adrenergic sensitivity following L6 spinal nerve ligation in monkey. J Neurophysiol 1999;81(2):455-466.

[2] Amin EM, Oltean S, Hua J, Gammons MV, Hamdollah-Zadeh M, Welsh GI, Cheung MK, Ni L, Kase S, Rennel ES, Symonds KE, Nowak DG, Royer-Pokora B, Saleem MA, Hagiwara M, Schumacher VA, Harper SJ, Hinton DR, Bates DO, Ladomery MR. WT1 mutants reveal SRPK1 to be a downstream angiogenesis target by altering VEGF splicing. Cancer cell 2011;20(6):768-780.

[3] Asadi S, Javan M, Ahmadiani A, Sanati MH. Alternative splicing in the synaptic protein interaction site of rat Ca(v)2.2 (alpha (1B)) calcium channels: changes induced by chronic inflammatory pain. Journal of molecular neuroscience : MN 2009;39(1-2):40-48.

[4] Ballmer-Hofer K, Andersson AE, Ratcliffe LE, Berger P. Neuropilin-1 promotes VEGFR-2 trafficking through Rab11 vesicles thereby specifying signal output. Blood 2011;118(3):816-826.

[5] Baron R, Janig W, Kollmann W. Sympathetic and afferent somata projecting in hindlimb nerves and the anatomical organization of the lumbar sympathetic nervous system of the rat. J Comp Neurol 1988;275(3):460-468.

[6] Bates D, Cui T, Doughty J, Winkler M, Sugiono M, Shields J, Peat D, Gillatt D, Harper S. VEGF165b, an inhibitory splice variant of vascular endothelial growth factor, is down-regulated in renal cell carcinoma. Cancer research 2002;62(15):4123-4131.

[7] Bates DO, Cui TG, Doughty JM, Winkler M, Sugiono M, Shields JD, Peat D, Gillatt D, Harper SJ. VEGF165b, an inhibitory splice variant of vascular endothelial growth factor, is down-regulated in renal cell carcinoma. Cancer research 2002;62(14):4123-4131.

[8] Bates DO, Mavrou A, Qiu Y, Carter JG, Hamdollah-Zadeh M, Barratt S, Gammons MV, Millar AB, Salmon AH, Oltean S, Harper SJ. Detection of VEGF-Axxxb Isoforms in Human Tissues. PLoS ONE 2013;8(7):e68399.

[9] Beazley-Long N, Hua J, Jehle T, Hulse RP, Dersch R, Lehrling C, Bevan H, Qiu Y, Lagreze WA, Wynick D, Churchill AJ, Kehoe P, Harper SJ, Bates DO, Donaldson LF. VEGF-A_{165}b Is an endogenous neuroprotective splice isoform of vascular endothelial growth factor A in vivo and in vitro. The American journal of pathology 2013;183(3):918-929.

[10] Bjork P, Jin S, Zhao J, Singh OP, Persson JO, Hellman U, Wieslander L. Specific combinations of SR proteins associate with single pre-messenger RNAs in vivo and contribute different functions. J Cell Biol 2009;184(4):555-568.

[11] Brumovsky P WM, Hökfelt T. Expression of the vesicular glutamate transporters-1 and -2 in adult mouse dorsal root ganglia and spinal cord and their regulation by nerve injury. Neuroscience 2007;147(2):469-490.

[12] Burger RA, Sill MW, Monk BJ, Greer BE, Sorosky JI. Phase II trial of bevacizumab in persistent or recurrent epithelial ovarian cancer or primary peritoneal cancer: a Gynecologic Oncology Group Study. J Clin Oncol 2007;25(33):5165-5171.

[13] Cébe Suarez S PM, Cariolato L, Arn S, Hoffmann U, Bogucki A, Manlius C, Wood J, Ballmer-Hofer K. A VEGF-A splice variant defective for heparan

sulfate and neuropilin-1 binding shows attenuated signaling through VEGFR-2. Cellular and molecular life sciences : CMLS 2006;63(17):2067-2077.

[14] Chen X, Levine JD. Mechanically-evoked C-fiber activity in painful alcohol and AIDS therapy neuropathy in the rat. Mol Pain 2007;3:5.

[15] Cheng JK, Ji RR. Intracellular signaling in primary sensory neurons and persistent pain. Neurochem Res 2008;33(10):1970-1978.

[16] Clark AK, Old EA, Malcangio M. Neuropathic pain and cytokines: current perspectives. J Pain Res 2013;6:803-814.

[17] Costes SV, Daelemans D, Cho EH, Dobbin Z, Pavlakis G, Lockett S. Automatic and quantitative measurement of protein-protein colocalization in live cells. Biophysical journal 2004;86(6):3993-4003.

[18] Costigan M, Scholz J, Woolf CJ. Neuropathic pain: a maladaptive response of the nervous system to damage. Annu Rev Neurosci 2009;32:1-32.

[19] Delestienne N, Wauquier C, Soin R, Dierick JF, Gueydan C, Kruys V. The splicing factor ASF/SF2 is associated with TIA-1-related/TIA-1-containing ribonucleoproteic complexes and contributes to post-transcriptional repression of gene expression. The FEBS journal 2010;277(11):2496-2514.

[20] Djouhri L, Koutsikou S, Fang X, McMullan S, Lawson SN. Spontaneous pain, both neuropathic and inflammatory, is related to frequency of spontaneous firing in intact C-fiber nociceptors. The Journal of neuroscience : the official journal of the Society for Neuroscience 2006;26(4):1281-1292.

[21] Donaldson LF, Beazley-Long N. Alternative RNA splicing: contribution to pain and potential therapeutic strategy. Drug discovery today 2016.

[22] Drake R, Hulse R, Lumb B, Donaldson L. The degree of acute descending control of spinal nociception in an area of primary hyperalgesia is dependent

on the peripheral domain of afferent input. The Journal of physiology 2014;592(16):3611-3624.

[23] Ferrari LF, Bogen O, Reichling DB, Levine JD. Accounting for the delay in the transition from acute to chronic pain: axonal and nuclear mechanisms. J Neurosci 2015;35(2):495-507.

[24] Fukuhara T, Hosoya T, Shimizu S, Sumi K, Oshiro T, Yoshinaka Y, Suzuki M, Yamamoto N, Herzenberg LA, Herzenberg LA, Hagiwara M. Utilization of host SR protein kinases and RNA-splicing machinery during viral replication. Proc Natl Acad Sci U S A 2006;103(30):11329-11333.

[25] Gammons MV, Fedorov O, D. I, Du C, Clark T, Hopkins C, Hagiwara M, Dick AD, Cox R, Harper SJ, Hancox JC, Knapp S, Bates D. Topical antiangiogenesis SRPK1 inhibitors reduce choroidal neovascularisation in rodent models of exudative AMD. IOVS 2013;54(9):6053.

[26] Gardell LR, Vanderah TW, Gardell SE, Wang R, Ossipov MH, Lai J, Porreca F. Enhanced evoked excitatory transmitter release in experimental neuropathy requires descending facilitation. The Journal of neuroscience : the official journal of the Society for Neuroscience 2003;23(23):8370-8379.

[27] Geranton SM, Jimenez-Diaz L, Torsney C, Tochiki KK, Stuart SA, Leith JL, Lumb BM, Hunt SP. A rapamycin-sensitive signaling pathway is essential for the full expression of persistent pain states. The Journal of neuroscience : the official journal of the Society for Neuroscience 2009;29(47):15017-15027.

[28] Ghosh G, Adams JA. Phosphorylation mechanism and structure of serine-arginine protein kinases. The FEBS journal 2011;278(4):587-597.

[29] Grosios K, Wood J, Esser R, Raychaudhuri A, Dawson J. Angiogenesis inhibition by the novel VEGF receptor tyrosine kinase inhibitor,

PTK787/ZK222584, causes significant anti-arthritic effects in models of rheumatoid arthritis. Inflamm Res 2004;53(4):133-142.

[30] Hargreaves K, Dubner R, Brown F, Flores C, Joris J. A new and sensitive method for measuring thermal nociception in cutaneous hyperalgesia. Pain 1988;32(1):77-88.

[31] Harper S, Bates D. VEGF-A splicing: the key to anti-angiogenic therapeutics? Nature reviews Cancer 2008;8(11):880-887.

[32] Hughes DI, Scott DT, Todd AJ, Riddell JS. Lack of evidence for sprouting of Abeta afferents into the superficial laminas of the spinal cord dorsal horn after nerve section. J Neurosci 2003;23(29):9491-9499.

[33] Hulse R, Wynick D, Donaldson L. Characterization of a novel neuropathic pain model in mice. Neuroreport 2008;19(8):825-829.

[34] Hulse R, Wynick D, Donaldson L. Intact cutaneous C fibre afferent properties in mechanical and cold neuropathic allodynia. European journal of pain 2010;14(6):565.

[35] Hulse RP, Beazley-Long N, Hua J, Kennedy H, Prager J, Bevan H, Qiu Y, Fernandes ES, Gammons MV, Ballmer-Hofer K, Gittenberger de Groot AC, Churchill AJ, Harper SJ, Brain SD, Bates DO, Donaldson LF. Regulation of alternative VEGF-A mRNA splicing is a therapeutic target for analgesia. Neurobiology of disease 2014;71:245-259.

[36] Hunt SP PA, Evan G. Induction of c-fos-like protein in spinal cord neurons following sensory stimulation. Nature 1987;328(6131):632-634.

[37] Kalsotra A, Cooper TA. Functional consequences of developmentally regulated alternative splicing. Nature reviews Genetics 2011;12(10):715-729.

[38] Khan GM, Chen SR, Pan HL. Role of primary afferent nerves in allodynia caused by diabetic neuropathy in rats. Neuroscience 2002;114(2):291-299.

[39] Kim HT PS, Lee SE, Chung JM, Lee DH. Non-noxious A fiber afferent input enhances capsaicin-induced mechanical hyperalgesia in the rat. Pain 2001;94(2):169-175.

[40] Kirillova I, Rausch VH, Tode J, Baron R, Janig W. Mechano- and thermosensitivity of injured muscle afferents. J Neurophysiol 2011;105(5):2058-2073.

[41] Koltzenburg M, Torebjork HE, Wahren LK. Nociceptor modulated central sensitization causes mechanical hyperalgesia in acute chemogenic and chronic neuropathic pain. Brain 1994;117 (Pt 3):579-591.

[42] Kramer HH, Doring K. Is the processing of low threshold mechanosensitive afferents altered in pain? Pain 2013;154(2):187-188.

[43] Langenberg MH, Witteveen PO, Roodhart J, Lolkema MP, Verheul HM, Mergui-Roelvink M, Brendel E, Kratzschmar J, Loembe B, Nol-Boekel A, Christensen O, Schellens JH, Voest EE. Phase I evaluation of telatinib, a VEGF receptor tyrosine kinase inhibitor, in combination with bevacizumab in subjects with advanced solid tumors. Ann Oncol 2011;22(11):2508-2515.

[44] Leith J, Wilson A, You H, Lumb B, Donaldson L. Periaqueductal grey cyclooxygenase-dependent facilitation of C-nociceptive drive and encoding in dorsal horn neurons in the rat. The Journal of physiology 2014;15(595):5093-5107.

[45] Leith JL, Wilson AW, Donaldson LF, Lumb BM. Cyclooxygenase-1-derived prostaglandins in the periaqueductal gray differentially control C- versus A-fiber-evoked spinal nociception. J Neurosci 2007;27(42):11296-11305.

[46] Li J, Simone D, Larson A. Windup leads to characteristics of central sensitization. Pain 1999;79(1):75-82.

[47] Li Q, Lau A, Morris TJ, Guo L, Fordyce CB, Stanley EF. A syntaxin 1, Galpha(o), and N-type calcium channel complex at a presynaptic nerve terminal: analysis by quantitative immunocolocalization. The Journal of neuroscience : the official journal of the Society for Neuroscience 2004;24(16):4070-4081.

[48] Liljencrantz J, Bjornsdotter M, Morrison I, Bergstrand S, Ceko M, Seminowicz DA, Cole J, Bushnell MC, Olausson H. Altered C-tactile processing in human dynamic tactile allodynia. Pain 2013;154(2):227-234.

[49] Lin J, Li G, Den X, Xu C, Liu S, Gao Y, Liu H, Zhang J, Li X, Liang S. VEGF and its receptor-2 involved in neuropathic pain transmission mediated by P2X(2)(/)(3) receptor of primary sensory neurons. Brain research bulletin 2010;83(5):284-291.

[50] Liu S, Xu C, Li G, Liu H, Xie J, Tu G, Peng H, Qiu S, Liang S. Vatalanib decrease the positive interaction of VEGF receptor-2 and P2X2/3 receptor in chronic constriction injury rats. Neurochemistry international 2012;60(6):565-572.

[51] Mavrou A, Brakspear K, Hamdollah-Zadeh M, Damodaran G, Babaei-Jadidi R, Oxley J, Gillatt D, Ladomery M, Harper S, Bates D, Oltean S. Serine-arginine protein kinase 1 (SRPK1) inhibition as a potential novel targeted therapeutic strategy in prostate cancer. Oncogene 2015;34(33):4311-4319.

[52] McCarthy KF CT, McCrory C. Cerebrospinal fluid levels of vascular endothelial growth factor correlate with reported pain and are reduced by spinal cord stimulation in patients with failed back surgery syndrome. Neuromodulation 2013;16(6):1525-1403.

[53] McMullan S, Simpson DA, Lumb BM. A reliable method for the preferential activation of C- or A-fibre heat nociceptors. Journal of neuroscience methods 2004;138(1-2):133-139.

[54] Minis A, Dahary D, Manor O, Leshkowitz D, Pilpel Y, Yaron A. Subcellular transcriptomics-dissection of the mRNA composition in the axonal compartment of sensory neurons. Developmental neurobiology 2014;74(3):365-381.

[55] Molander C, Hongpaisan J, Persson JK. Distribution of c-fos expressing dorsal horn neurons after electrical stimulation of low threshold sensory fibers in the chronically injured sciatic nerve. Brain Res 1994;644(1):74-82.

[56] Nakae A, Nakai K, Tanaka T, Hosokawa K, Mashimo T. Serotonin 2C receptor alternative splicing in a spinal cord injury model. Neuroscience letters 2013;532:49-54.

[57] Nesic O, Sundberg LM, Herrera JJ, Mokkapati VU, Lee J, Narayana PA. Vascular endothelial growth factor and spinal cord injury pain. J Neurotrauma 2010;27(10):1793-1803.

[58] Neumann S, Braz JM, Skinner K, Llewellyn-Smith IJ, Basbaum AI. Innocuous, not noxious, input activates PKCgamma interneurons of the spinal dorsal horn via myelinated afferent fibers. The Journal of neuroscience : the official journal of the Society for Neuroscience 2008;28(32):7936-7944.

[59] Nowak DG, Amin EM, Rennel ES, Hoareau-Aveilla C, Gammons M, Damodoran G, Hagiwara M, Harper SJ, Woolard J, Ladomery MR, Bates DO. Regulation of vascular endothelial growth factor (VEGF) splicing from pro-angiogenic to anti-angiogenic isoforms: a novel therapeutic strategy for angiogenesis. J Biol Chem 2010;285(8):5532-5540.

[60] Nowak DG, Woolard J, Amin EM, Konopatskaya O, Saleem MA, Churchill AJ, Ladomery MR, Harper SJ, Bates DO. Expression of pro- and anti-angiogenic isoforms of VEGF is differentially regulated by splicing and growth factors. Journal of cell science 2008;121(Pt 20):3487-3495.

[61] Obara I, Hunt SP. Axonal protein synthesis and the regulation of primary afferent function. Developmental neurobiology 2014;74(3):269-278.

[62] Oliveira AL, Hydling F, Olsson E, Shi T, Edwards RH, Fujiyama F, Kaneko T, Hokfelt T, Cullheim S, Meister B. Cellular localization of three vesicular glutamate transporter mRNAs and proteins in rat spinal cord and dorsal root ganglia. Synapse 2003;50(2):117-129.

[63] Oltean S, Qiu Y, Ferguson J, Stevens M, Neal C, Russell A, Kaura A, Arkill K, Harris K, Symonds C, Lacey K, Wijeyaratne L, Gammons M, Wylie E, Hulse R, Alsop C, Cope G, Damodaran G, Betteridge K, Ramnath R, Satchell S, Foster R, Ballmer-Hofer K, Donaldson L, Barratt J, Baelde H, Harper S, Bates D, Salmon A. Vascular Endothelial Growth Factor-A165b Is Protective and Restores Endothelial Glycocalyx in Diabetic Nephropathy. J Am Soc Nephrol 2014;26(8):1889-1904.

[64] Phillips LH, 2nd, Park TS. Electrophysiological mapping of the segmental innervation of the saphenous and sural nerves. Muscle & nerve 1993;16(8):827-831.

[65] Ropper AH, Gorson KC, Gooch CL, Weinberg DH, Pieczek A, Ware JH, Kershen J, Rogers A, Simovic D, Schratzberger P, Kirchmair R, Losordo D. Vascular endothelial growth factor gene transfer for diabetic polyneuropathy: a randomized, double-blinded trial. Ann Neurol 2009;65(4):386-393.

[66] Saab CY. Pain-related changes in the brain: diagnostic and therapeutic potentials. Trends Neurosci 2012;35(10):629-637.

[67] Schneider C, Rasband W, Eliceiri K. NIH Image to ImageJ: 25 years of image analysis. Nat Methods 2012;9(7):671-675.

[68] Serra J, Bostock H, Sola R, Aleu J, Garcia E, Cokic B, Navarro X, Quiles C. Microneurographic identification of spontaneous activity in C-nociceptors in neuropathic pain states in humans and rats. Pain 2012;153(1):42-55.

[69] Serra J, Collado A, Sola R, Antonelli F, Torres X, Salgueiro M, Quiles C, Bostock H. Hyperexcitable C nociceptors in fibromyalgia. Ann Neurol 2014;75(2):196-208.

[70] Shim B, Ringkamp M, Lambrinos GL, Hartke TV, Griffin JW, Meyer RA. Activity-dependent slowing of conduction velocity in uninjured L4 C fibers increases after an L5 spinal nerve injury in the rat. Pain 2007;128(1-2):40-51.

[71] Sondell M LG, Kanje M. Vascular endothelial growth factor has neurotrophic activity and stimulates axonal outgrowth, enhancing cell survival and Schwann cell proliferation in the peripheral nervous system. J Neurosci 1999;19(14):5731-5740.

[72] Sondell M, Sundler F, Kanje M. Vascular endothelial growth factor is a neurotrophic factor which stimulates axonal outgrowth through the flk-1 receptor. Eur J Neurosci 2000;12(12):4243-4254.

[73] Tavares R, Scherer N, Ferreira C, Costa F, Passetti F. Splice variants in the proteome: a promising and challenging field to targeted drug discovery. Drug Discov Today 2015;20(3):353-360.

[74] Torebjörk H, Lundberg L, LaMotte R. Central changes in processing of mechanoreceptive input in capsaicin-induced secondary hyperalgesia in humans. The Journal of physiology 1992;448:765-780.

[75] Torsney C. Inflammatory pain unmasks heterosynaptic facilitation in lamina I neurokinin 1 receptor-expressing neurons in rat spinal cord. J Neurosci 2011;31(13):5158-5168.

[76] Torsney C. Inflammatory pain unmasks heterosynaptic facilitation in lamina I neurokinin 1 receptor-expressing neurons in rat spinal cord. The Journal of neuroscience : the official journal of the Society for Neuroscience 2011;31(13):5158-5168.

[77] Tripathi V, Song DY, Zong X, Shevtsov SP, Hearn S, Fu XD, Dundr M, Prasanth KV. SRSF1 regulates the assembly of pre-mRNA processing factors in nuclear speckles. Molecular biology of the cell 2012;23(18):3694-3706.

[78] Tsantoulas C, McMahon SB. Opening paths to novel analgesics: the role of potassium channels in chronic pain. Trends in neurosciences 2014;37(3):146-158.

[79] Tsantoulas C, Zhu L, Shaifta Y, Grist J, Ward JP, Raouf R, Michael GJ, McMahon SB. Sensory neuron downregulation of the Kv9.1 potassium channel subunit mediates neuropathic pain following nerve injury. J Neurosci 2012;32(48):17502-17513.

[80] Uceyler N, Sommer C. Cytokine regulation in animal models of neuropathic pain and in human diseases. Neurosci Lett 2008;437(3):194-198.

[81] Ueda H. Molecular mechanisms of neuropathic pain-phenotypic switch and initiation mechanisms. Pharmacol Ther 2006;109(1-2):57-77.

[82] van Neerven S, Joosten EA, Brook GA, Lambert CA, Mey J, Weis J, Marcus MA, Steinbusch HW, van Kleef M, Patijn J, Deumens R. Repetitive intrathecal VEGF(165) treatment has limited therapeutic effects after spinal cord injury in the rat. J Neurotrauma 2010;27(10):1781-1791.

[83] Verheyen A, Peeraer E, Nuydens R, Dhondt J, Poesen K, Pintelon I, Daniels A, Timmermans JP, Meert T, Carmeliet P, Lambrechts D. Systemic anti-vascular endothelial growth factor therapies induce a painful sensory neuropathy. Brain 2012;135(Pt 9):2629-2641.

[84] Walczak JS, Pichette V, Leblond F, Desbiens K, Beaulieu P. Behavioral, pharmacological and molecular characterization of the saphenous nerve partial ligation: a new model of neuropathic pain. Neuroscience 2005;132(4):1093-1102.

[85] Whittles CE, Pocock TM, Wedge SR, Kendrew J, Hennequin LF, Harper SJ, Bates DO. ZM323881, a novel inhibitor of vascular endothelial growth factor-receptor-2 tyrosine kinase activity. Microcirculation 2002;9(6):513-522.

[86] Wood JM, Bold G, Buchdunger E, Cozens R, Ferrari S, Frei J, Hofmann F, Mestan J, Mett H, O'Reilly T, Persohn E, Rosel J, Schnell C, Stover D, Theuer A, Towbin H, Wenger F, Woods-Cook K, Menrad A, Siemeister G, Schirner M, Thierauch KH, Schneider MR, Drevs J, Martiny-Baron G, Totzke F. PTK787/ZK 222584, a novel and potent inhibitor of vascular endothelial growth factor receptor tyrosine kinases, impairs vascular endothelial growth factor-induced responses and tumor growth after oral administration. Cancer research 2000;60(8):2178-2189.

[87] Woodbury CJ, Kullmann FA, McIlwrath SL, Koerber HR. Identity of myelinated cutaneous sensory neurons projecting to nocireceptive laminae following

nerve injury in adult mice. The Journal of comparative neurology 2008;508(3):500-509.

[88] Woolard J, Wang WY, Bevan HS, Qiu Y, Morbidelli L, Pritchard-Jones RO, Cui TG, Sugiono M, Waine E, Perrin R, Foster R, Digby-Bell J, Shields JD, Whittles CE, Mushens RE, Gillatt DA, Ziche M, Harper SJ, Bates DO. VEGF165b, an inhibitory vascular endothelial growth factor splice variant: mechanism of action, in vivo effect on angiogenesis and endogenous protein expression. Cancer research 2004;64(21):7822-7835.

[89] Woolf C, King A. Dynamic alterations in the cutaneous mechanoreceptive fields of dorsal horn neurons in the rat spinal cord. The Journal of neuroscience : the official journal of the Society for Neuroscience 1990;10(8):2717-2726.

[90] Woolf CJ. Central sensitization: implications for the diagnosis and treatment of pain. Pain 2011;152(3 Suppl):S2-15.

[91] Woolf CJ, Shortland P, Coggeshall RE. Peripheral nerve injury triggers central sprouting of myelinated afferents. Nature 1992;355(6355):75-78.

[92] Yasaka T, Tiong SY, Polgar E, Watanabe M, Kumamoto E, Riddell JS, Todd AJ. A putative relay circuit providing low-threshold mechanoreceptive input to lamina I projection neurons via vertical cells in lamina II of the rat dorsal horn. Molecular pain 2014;10:3.

[93] Yeomans D, Pirec V, Proudfit H. Nociceptive responses to high and low rates of noxious cutaneous heating are mediated by different nociceptors in the rat: behavioral evidence. Pain 1996;68(1):133-140.

[94] Yeomans D, Proudfit H. Nociceptive responses to high and low rates of noxious cutaneous heating are mediated by different nociceptors in the rat: electrophysiological evidence. Pain 1996;68(1):141-150.

[95] Zhong Y, Banning AS, Cockayne DA, Ford AP, Burnstock G, McMahon SB. Bladder and cutaneous sensory neurons of the rat express different functional P2X receptors. Neuroscience 2003;120(3):667-675.

[96] Zhu YF, Henry JL. Excitability of Abeta sensory neurons is altered in an animal model of peripheral neuropathy. BMC neuroscience 2012;13:15.

[97] Ziegler EA, Magerl R, R.A. M, R.D. T. Secondary hyperalgesia to punctate mechanical stimuli. Brain : a journal of neurology 1999;122:2245-2257.

[98] Ziegler EA, Magerl W, Meyer RA, Treede RD. Secondary hyperalgesia to punctate mechanical stimuli. Central sensitization to A-fibre nociceptor input. Brain 1999;122 (Pt 12):2245-2257.

Figures and Legends

Figure 1. SRSF1 expression and activation in DRG sensory neurons following PSNI injury

[A-C] SRSF1 (Red) was expressed in the cytoplasm (not co-localized with DAPI) of the DRG sensory neurons in naïve animals. [D] Replacement of the primary antibody with a species matched IgG control DRG image resulted in no staining. [E-G] SRSF1 was co-localized with nuclear stain DAPI in DRG sensory neurons following PSNI injury (arrows). In some neurons cytoplasmic SRSF1 is still evident (arrowheads). [H] Omission of the primary antibody resulted in no staining. [I & J] Representative examples of ATF3 expression in NeuN-co-labeled DRG sensory neurons in [I] naïve and [J] PSNI animals. [K] The number of ATF3 positive DRG neurons was significantly increased in the L4 from PSNI animals (unpaired t test, n=5/group). [L-O] High magnification representative images of SRSF1/ATF3/NeuN co-labeled DRG neurons. (white arrows). ** $p<0.001$. Scale bars = 50µm low magnification and 20µm high magnification.

Figure 2. SRSF1 expression in NF200 sensory neurons

[A-C] SRSF1 expression in the cytoplasm of NF-200-positive L4 dorsal root ganglia neurons in the naïve animal. [C] Note the clear cytoplasmic localization of the SRSF1 (arrows). [D-F] Following PSNI, clear SRSF1 nuclear translocation was evident in the NF200 positive neurons (arrows in F). [G] SRSF1 was not expressed in IB4 positive dorsal root ganglia neurons, [H] though SRSF1 is co-localized with nuclear marker DAPI. [I-K] SRSF1 was also localized to NF200-rich sensory nerve

fibers of the PSNI saphenous nerve. [L] Quantification of the SRSF1 positive and total number of sensory neurons in the dorsal root ganglia by cell cross-sectional area (μm^2) in naïve and PSNI injured rats. Scale bars = 50µm. N=5 per group.

Figure 3. SRSF1 is expressed in myelinated central terminals in the dorsal horn of the spinal cord and increased after PSNI

[A] SRSF1 was expressed at low levels in the dorsal horn of the spinal cord in naïve animals. [B] vGLUT1 was used as a marker of myelinated sensory fiber central terminals. [C] Merged image of SRSF1 and vGLUT1. [D-F] Two days after PSNI nerve injury there was an increase of SRSF1 expression in the spinal cord, still co-localized with vGLUT1. [F] Inset images of no primary SRSF1 (i) and vGlut1 (ii) antibodies. [G-I] High power views of boxes marked in D-F. [J] Increased SRSF1 expression/localization within the lumbar spinal cord following PSNI was demonstrated by western blot with two different primary antibodies (Santa Cruz mouse monoclonal and Abcam rabbit polyclonal antibodies). [K] Quantification of increased expression post-PSNI in spinal cord vs. naïve rats (Abcam antibody, Mann Whitney U test, $p=0.055$, n=3) [L] Using coloc2 analysis through determination of Pearson correlation coefficient, there was an increase in the degree of co-localization between vGLUT1 and SRSF1 immunoreactivity in the spinal cord following PSNI, compared to naïve (**$p<0.01$ Mann Whitney test, n=4 per group). [M] SRSF1 was expressed in DRG neurons that were [N] positive for vGLUT1, a marker of excitatory large diameter DRG neurons. [O] Overlay of vGLUT1 and SRSF1 images. [P & Q] Representative images of SRSF1 stained spinal cord sections used for analysis, showing the contralateral dorsal horn from [P] a naïve and [Q] PSNI

animal. [R & S] The same images of contralateral dorsal horns showing VGLUT1 staining in [R] naïve and [S] PSNI animals (Scale bars = 50µm).

Figure 4. $VEGF_{xxx}a$ isoform expression increases in the spinal cord following PSNI.

[A-F] Immunofluorescence of VEGF in the naïve ([A] ipsilateral [B] contralateral), PSNI ([C] ipsilateral [D] contralateral) and PSNI+SRPIN ([E] ipsilateral [F] contralateral) spinal cord (superficial dorsal horn located in top right of images) using the pan-VEGF-A antibody A20. [G-I] Co-localization of pan-VEGF-A with SRSF1 in the dorsal horn of the lumbar spinal cord (high magnification images). [J] Western blot of protein extracted from spinal cords of 6 animals, three naïve and three after PSNI. Pan-VEGF-A but not $VEGF\text{-}A_{165}b$ increased after PSNI. [K]. Densitometric analysis of the Western blot showed a large increase in pan-VEGF-A expression, no increase in $VEGF\text{-}A_{xxx}b$ expression and [L] a reduction in the proportion of $VEGF\text{-}A_{xxx}b$ after PSNI versus naïve animals (one way ANOVA, Sidak post hoc test, *$p<0.05$, ($F(3,6)=1.347$), n=3 per group). Scale bars = 50µm.

Figure 5. Inhibition of SRPK1 activity in the spinal cord prevents neuropathic pain

Intrathecal (i.t.) SRPIN340 treatment in rats completely prevented [A] mechanical (F test (2,20) = 3.539), [B] dynamic brush allodynia (F (2,20) = 5.526) and [C] cooling allodynia (F (2, 20) = 7.8) after PSNI (n=9, PSNI + vehicle, n=6, PSNI + SRPIN340) in the ipsilateral hindpaw. Contralateral hind-paws were not different between groups following mechanical, brush and cooling nociceptive testing. Withdrawal latencies were increased both [D] ipsilaterally (F(2,20) = 25.86) and [E] contralaterally (F(2,

20) = 12.72) following i.t. SRPIN340 treatment. (*p<0.05, **p<0.01, ***p<0.001 two way ANOVA with post-hoc Bonferroni tests).

Figure 6. PSNI increases and intrathecal SRPIN340 reduces SRSF1 expression in the spinal dorsal horn.

[A-C] SRSF1 immunoreactivity in vGLUT1-positive terminals in the spinal cord after PSNI. (C shows the co-localization of SRSF1 and vGLUT1). [D-F] Intrathecal 10µM SRPIN340 reduced SRSF1 immunoreactivity in vGLUT1-positive terminals. [F] indicates that there is a loss of expression of SRSF1 but not vGLUT-1. [G] Quantification of SRSF1/vGLUT1 fluorescence intensity by area. PSNI increased SRSF1 staining and SRPIN340 treatment led to a reduction in SRSF1 immunostaining within the dorsal horn 2 days after PSNI ($F_{(2,9)}$ =11.16, *p<0.05, **p<0.01 one way ANOVA with post-hoc Bonferroni test; n=4 per group). [H] Intrathecal SRPIN 340 treatment in PSNI injured animals demonstrate a reduction in colocalisation between vGLUT1 and SRSF1 compared to PSNI+vehicle group (**p<0.01, Mann Whitney test, n=4 per group).

Figure 7. Inhibition of SRPK1 in the spinal cord following PSNI leads to reduction in VEGF-A_{xxx}a expression.

[A] Immunoblotting for pan-VEGF-A, VEGF-A_{xxx}b and tubulin expression in spinal cord from 4 PSNI animals treated with vehicle or SRPIN340. [B] Quantification of intensity showed that the amount of VEGF-A_{xxx}b increased slightly, and pan-VEGF-A reduced resulting in [C] a restoration of the VEGF-A_{165}b ratio in PSNI towards that in

naïve control animals (compare with Fig. 3H, one way ANOVA, *p<0.05 Sidak test (F(3,6)=3.529) n=3 per group). [D-E] C-fos immunostaining in spinal cord dorsal horn in PSNI animals treated with either i.t. vehicle or SRPIN340. [F]. Increased spinal neuronal activation, indicated by increased numbers of c-fos expressing dorsal horn neurons after PSNI, was blocked by PSNI+SRPIN340 treatment (one way ANOVA with post Bonferroni test, *** p<0.001, (F(2, 9) = 36.50), n=4 per group for c-fos expression). [G] SRPK1 was expressed in the lumbar spinal cord in the naïve animal, and was unchanged post-PSNI (n=3 per group, NS) Scale bar=40μm.

Figure 8. VEGF receptor 2 blockade leads to attenuation of nociceptive pain behavior in rats.

[A] Intraperitoneal injection of 30mg/kg PTK787 led to an increased withdrawal latency to heat (two way ANOVA with post-hoc Bonferroni test n=5/group, **p<0.01, (F(1,20) = 5.388). Intraperitoneal 30mg/kg PTK787 attenuated both [B] time (F (11, 132) = 13.39) and [C] number (F)11, 132) = 4.015) of formalin-induced pain behaviors within the second phase (two way ANOVA with post-hoc Bonferroni test, *p<0.05, **p<0.01, n=7/group). Area under the curve analysis of [D] duration (F(1,12) = 5.874) and [E] number (F (1,12) = 8.739) for the two phases of nociceptive behaviors shown in B & C (**p<0.01, ***p<0.001 two way ANOVA with post-hoc Bonferroni test). [F] Intrathecal injection of 200nM of VEGFR2 antagonist ZM323881 led to an increase in EMG response threshold only to A-nociceptor stimulation versus baseline and vehicle groups (**p<0.01; two way ANOVA with post Bonferroni) (n=3-5/group).

Figure 9. Alteration of spinal VEGFR activation attenuates nociceptive behavior in naïve mice and rats

[A] Intrathecal administration of 200nM PTK787 increased mechanical withdrawal thresholds ($F(1,10) = 12.47$) and [B] increased withdrawal latency to heat in mice ($F(1, 12) = 8.165$, n=4/group vehicle, (8 hind paws used as replicates), n=3/group PTK787, (6 hind paws used as replicates), $^{**}p<0.01$ two-way ANOVA with post-hoc Bonferroni test). [C] Intrathecal VEGF-A_{165}a reduced mechanical thresholds ($F(1,12) = 17.18$) and [D] heat ($F(1,12) = 18.61$) withdrawal latencies in mice (n=4/group (8 hind paws used as replicates). [E] Intrathecal VEGF-A_{165}b increased mechanical thresholds ($F(1,12) = 25.26$) and [F] thermal ($F(1,16) = 5.631$) response latencies in mice (n=4 vehicle group (8 hind paws used as replicates), n=5 VEGF group, (10 hind paws used as replicates)). [G] Treatment of rats with a VEGF-A_{165}b neutralizing antibody decreased both mechanical thresholds ($F(1, 15) = 18.66$) and [H] thermal latencies (($F(1,15) = 1.400$, n=3 group (6 hind paws used as replicates), two way ANOVA with post-hoc Bonferroni test, $^{***}p<0.001$).

Figure 10. Attenuation of VEGFR2 signaling leads to alleviation of neuropathic pain in rats

Intrathecal application of VEGF-A_{165}b two days after PSNI surgery abolished [A] mechanical ($F(2, 10) = 32.39$) and [B] cooling ($F(2, 20) = 14.03$) allodynia (n=6 per group), and increased withdrawal latencies to heat in both [C] ipsilateral ($F(2,20) = 4.201$) and [D] contralateral hind paws ($F(2,10) = 3.476$, two way ANOVA with post-hoc Bonferroni test, $^{*}p<0.05$, $^{**}p<0.01$, $^{***}p<0.001$, n=6 per group). Contralateral hind-paws from both groups did not differ in nociceptive behavioral response to [A]

mechanical and [B] cooling stimulation. IP 30mg/kg PTK787 led to increased withdrawal latencies to heat in the [E] ipsilateral ($F(2,12)=2.45$) and [F] contralateral limb ($F(2,12)=1.38$)) (two way ANOVA with post-hoc Bonferroni test, $^{**}p<0.01$, n=4 per group).

Figure. 1

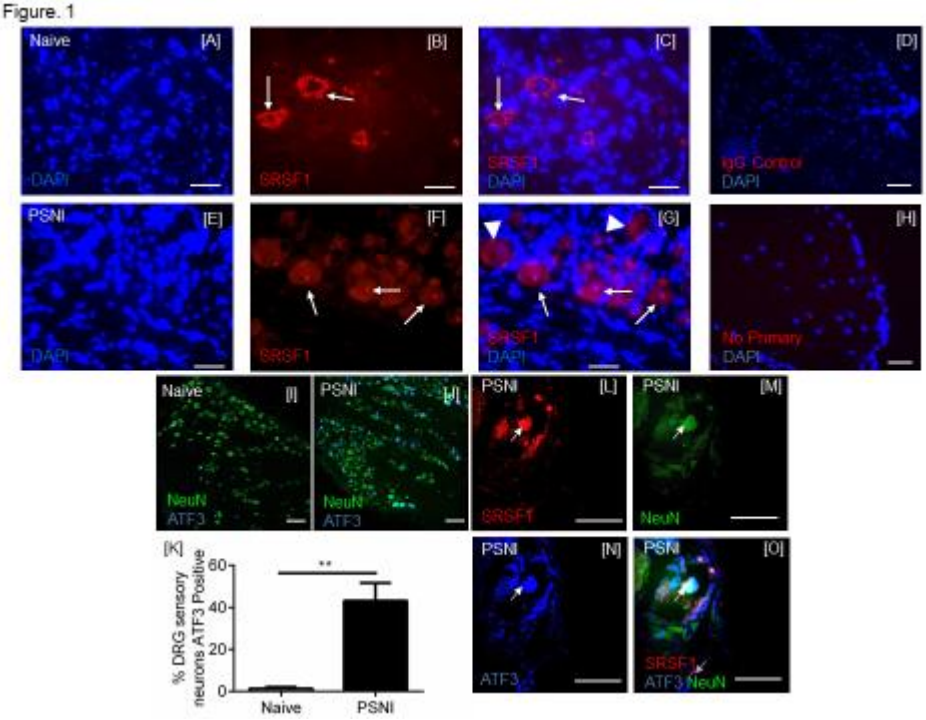
Naive
[A]
DAPI
[B]
SRSF1
[C]
SRSF1
DAPI
[D]
IgG Control
DAPI
PSNI
[E]
DAPI
[F]
SRSF1
[G]
SRSF1
DAPI
[H]
No Primary
DAPI
Naive
[I]
NeuN
ATF3
PSNI
[J]
NeuN
ATF3
PSNI
[L]
SRSF1
PSNI
[M]
NeuN
[K]
% DRG sensory neurons ATF3 Positive
60
40
20
0
**
Naive
PSNI
PSNI
[N]
ATF3
PSNI
[O]
SRSF1
ATF3 NeuN

1

2

Figure. 2

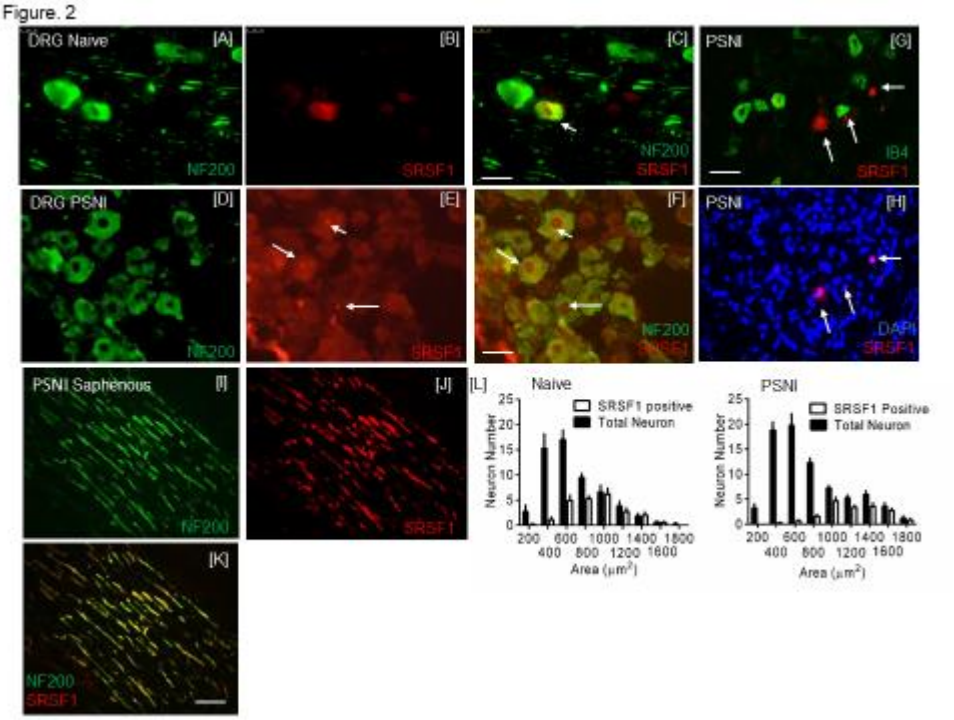
DRG Naive
[A]
NF200
[B]
SRSF1
[C]
NF200
SRSF1
PSNI
[G]
IB4
SRSF1
DRG PSNI
[D]
NF200
[E]
SRSF1
[F]
NF200
SRSF1
PSNI
[H]
DAPI
SRSF1
PSNI Saphenous
[I]
NF200
[J]
SRSF1
[K]
NF200
SRSF1
[L]
Naive
SRSF1 positive
Total Neuron
Neuron Number
Area (μm²)
PSNI
SRSF1 Positive
Total Neuron
Neuron Number
Area (μm²)

1

2

Figure. 3

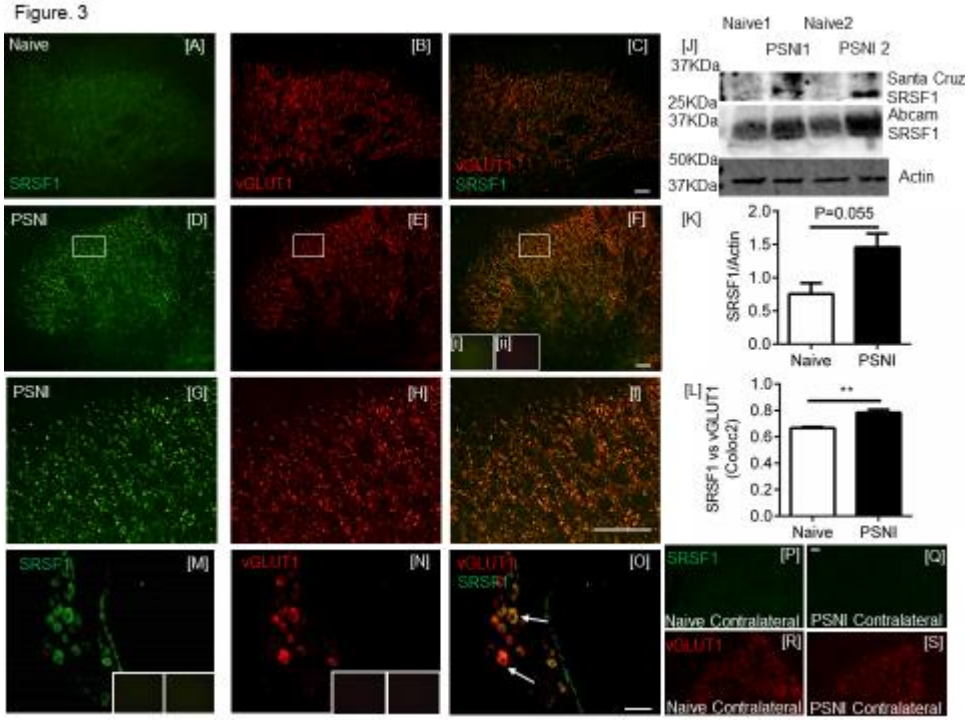
Naive
[A]
SRSF1
[B]
vGLUT1
[C]
vGLUT1
SRSF1
PSNI
[D]
[E]
[F]
[i]
[ii]
PSNI
[G]
[H]
[I]
SRSF1
[M]
vGLUT1
[N]
vGLUT1
SRSF1
[O]
[J]
Naive1
Naive2
PSNI1
PSNI 2
37KDa
Santa Cruz
SRSF1
25KDa
37KDa
Abcam
SRSF1
50KDa
37KDa
Actin
[K]
P=0.055
SRSF1/Actin
2.0
1.5
1.0
0.5
0.0
Naive
PSNI
[L]
**
SRSF1 vs vGLUT1 (Coloc2)
1.0
0.8
0.6
0.4
0.2
0.0
Naive
PSNI
SRSF1
[P]
[Q]
Naive Contralateral
PSNI Contralateral
vGLUT1
[R]
[S]
Naive Contralateral
PSNI Contralateral

1

2

Figure. 4

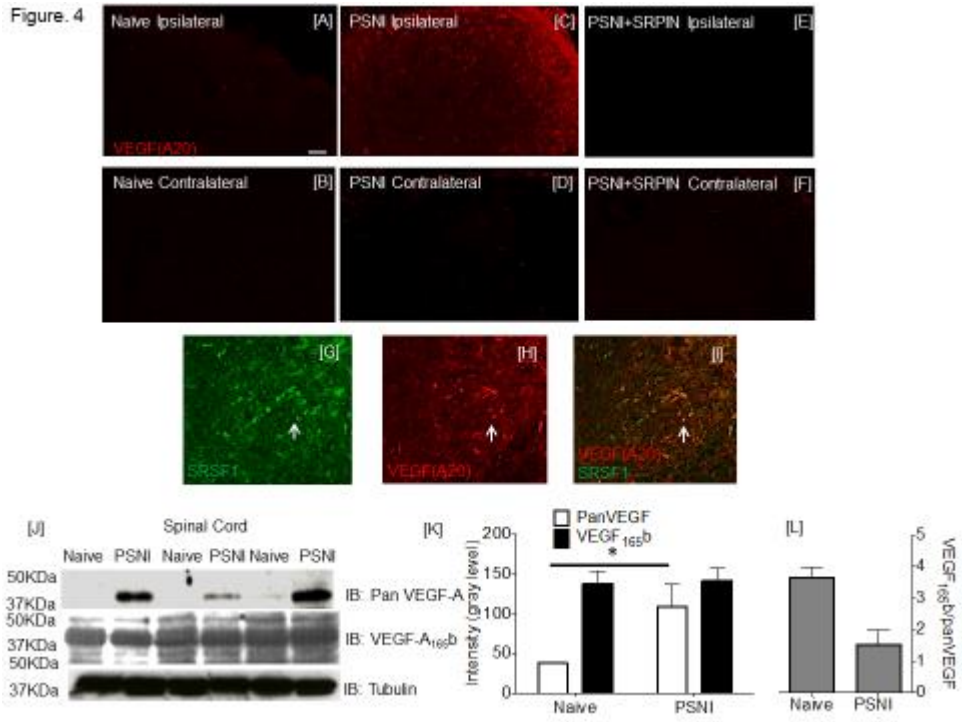
Naive Ipsilateral
[A]
PSNI Ipsilateral
[C]
PSNI+SRPIN Ipsilateral
[E]
Naive Contralateral
[B]
PSNI Contralateral
[D]
PSNI+SRPIN Contralateral
[F]
[G]
SRSF1
[H]
VEGF(A20)
[I]
[J]
Spinal Cord
Naive PSNI Naive PSNI Naive PSNI
50KDa
37KDa
50KDa
37KDa
50KDa
37KDa
IB: Pan VEGF-A
IB: VEGF-A165b
IB: Tubulin
[K]
PanVEGF
VEGF165b
*
Intensity (gray level)
200
150
100
50
0
Naive
PSNI
[L]
5
4
3
2
1
0
VEGF165b/panVEGF
Naive
PSNI

1

2

Figure. 5

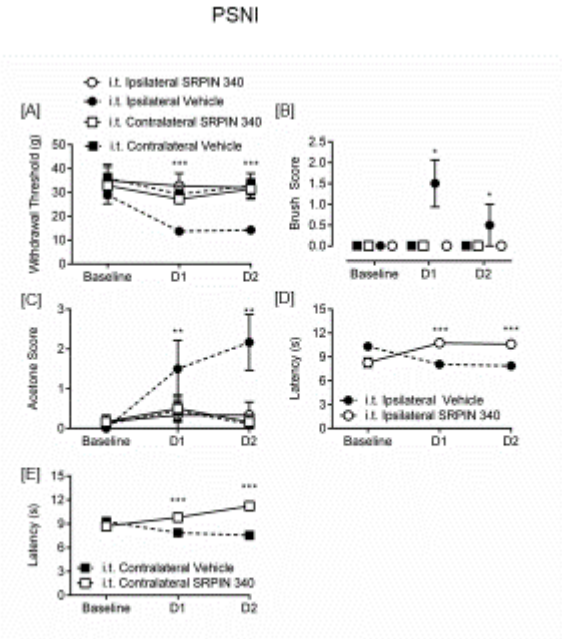
PSNI
i.t. Ipsilateral SRPIN 340
i.t. Ipsilateral Vehicle
i.t. Contralateral SRPIN 340
i.t. Contralateral Vehicle
[A]
Withdrawal Threshold (g)
Baseline
D1
D2
[B]
Brush Score
[C]
Acetone Score
[D]
Latency (s)
[E]
Latency (s)

1

2

Figure. 6

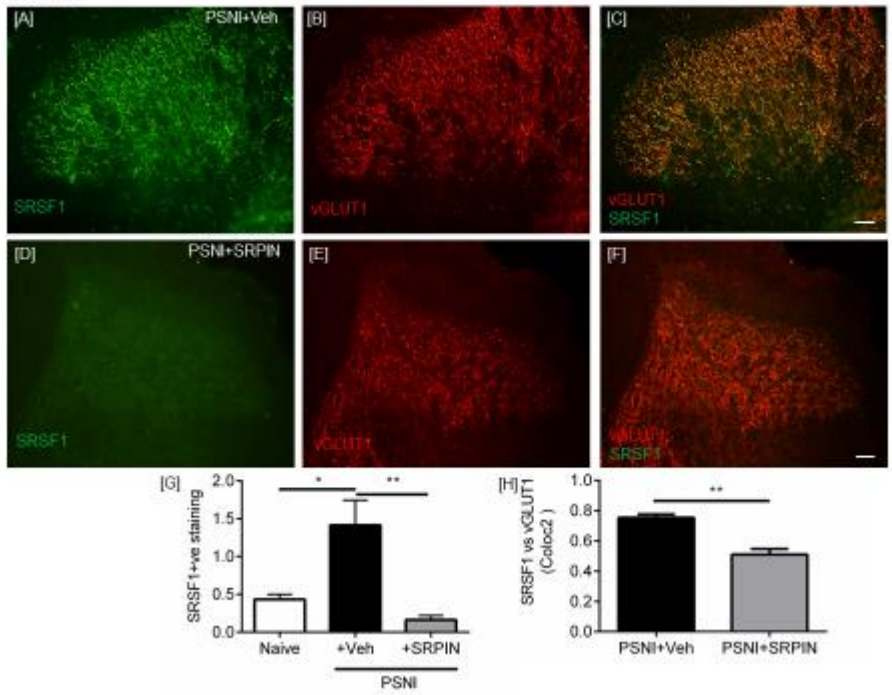
[A]
PSNI+Veh
SRSF1
[B]
vGLUT1
[C]
vGLUT1
SRSF1
[D]
PSNI+SRPIN
SRSF1
[E]
vGLUT1
[F]
vGLUT1
SRSF1
[G]
SRSF1+ve staining
2.0
1.5
1.0
0.5
0.0
*
**
Naive
+Veh
+SRPIN
PSNI
[H]
SRSF1 vs vGLUT1 (Coloc2)
1.0
0.8
0.6
0.4
0.2
0.0
**
PSNI+Veh
PSNI+SRPIN

1

2

Figure. 7

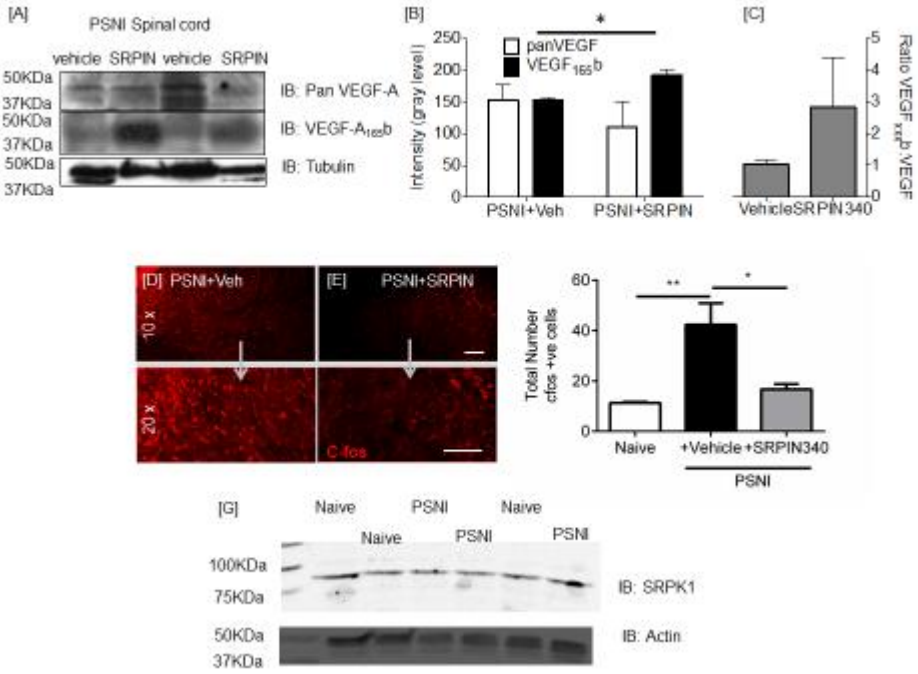
[A]
PSNI Spinal cord
vehicle SRPIN vehicle SRPIN
50KDa
37KDa
50KDa
37KDa
50KDa
37KDa
IB: Pan VEGF-A
IB: VEGF-A165b
IB: Tubulin
[B]
panVEGF
VEGF165b
Intensity (gray level)
PSNI+Veh
PSNI+SRPIN
[C]
Ratio VEGFxxxb/VEGF
Vehicle
SRPIN340
[D] PSNI+Veh
[E] PSNI+SRPIN
10 x
20 x
C-fos
Total Number cfos +ve cells
Naive
+Vehicle
+SRPIN340
PSNI
[G]
Naive
PSNI
Naive
Naive
PSNI
PSNI
100KDa
75KDa
50KDa
37KDa
IB: SRPK1
IB: Actin

1

2

Figure. 8

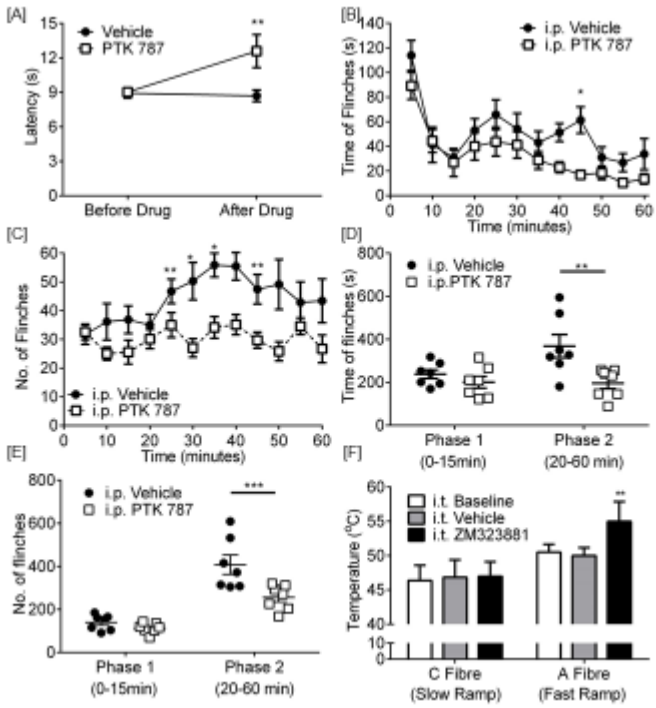
[A]
Vehicle
PTK 787
Latency (s)
Before Drug
After Drug
[B]
i.p. Vehicle
i.p. PTK 787
Time of Flinches (s)
Time (minutes)
[C]
No. of Flinches
i.p. Vehicle
i.p. PTK 787
Time (minutes)
[D]
i.p. Vehicle
i.p.PTK 787
Time of flinches (s)
Phase 1
(0-15min)
Phase 2
(20-60 min)
[E]
i.p. Vehicle
i.p. PTK 787
No. of flinches
Phase 1
(0-15min)
Phase 2
(20-60 min)
[F]
i.t. Baseline
i.t. Vehicle
i.t. ZM323881
Temperature (°C)
C Fibre
(Slow Ramp)
A Fibre
(Fast Ramp)

1

2

Figure. 9

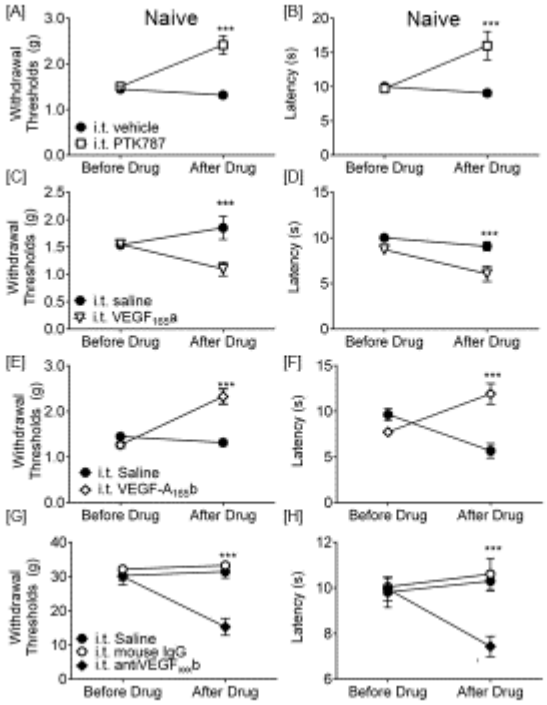
[A]
Naive
Withdrawal Thresholds (g)
i.t. vehicle
i.t. PTK787
Before Drug
After Drug
***
[B]
Naive
Latency (s)
Before Drug
After Drug
***
[C]
Withdrawal Thresholds (g)
i.t. saline
i.t. VEGF$_{165}$a
Before Drug
After Drug
***
[D]
Latency (s)
Before Drug
After Drug
***
[E]
Withdrawal Thresholds (g)
i.t. Saline
i.t. VEGF-A$_{165}$b
Before Drug
After Drug
***
[F]
Latency (s)
Before Drug
After Drug
***
[G]
Withdrawal Thresholds (g)
i.t. Saline
i.t. mouse IgG
i.t. antiVEGF$_{165}$b
Before Drug
After Drug
***
[H]
Latency (s)
Before Drug
After Drug
***

1

2

Figure. 10

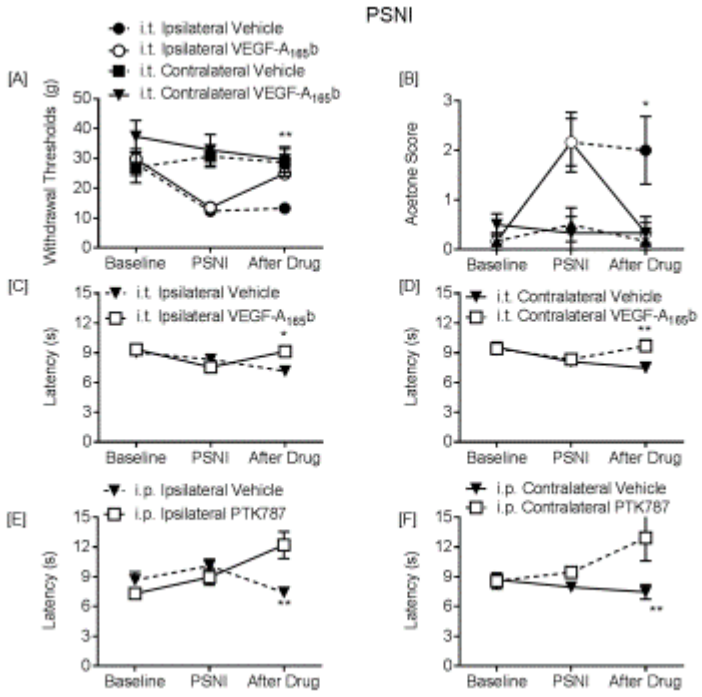
PSNI
[A]
i.t. Ipsilateral Vehicle
i.t. Ipsilateral VEGF-A165b
i.t. Contralateral Vehicle
i.t. Contralateral VEGF-A165b
Withdrawal Thresholds (g)
Baseline
PSNI
After Drug
[B]
Acetone Score
[C]
Latency (s)
[D]
[E]
i.p. Ipsilateral Vehicle
i.p. Ipsilateral PTK787
[F]
i.p. Contralateral Vehicle
i.p. Contralateral PTK787

1